Tornadogenesis in High-end Tornadic Supercells (Part 1)
The RFD Surge, RFD Occlusion and Cell Mergers

Chris Broyles[1], Corey Potvin[2], Greg Dial[1], James Murnan[2], Steven Shores[4], Andrew Lyons[1], Matthew Elliott[1], Ashton Robinson Cook[3]

[1] NOAA/NWS/NCEP/Storm Prediction Center, Norman, Oklahoma
[2] NOAA/National Severe Storms Laboratory, Norman, Oklahoma
[3] Weather Prediction Center, [4] University of Oklahoma Student

Abstract

A database of 208 supercells that produced tornadoes rated EF3 to EF5, was created at the Storm Prediction Center to collect data on observational features involved in high-end tornadogenesis. Using WSR-88D high-resolution radar, a rear-flank downdraft (RFD) surge and an RFD occlusion were identified just prior to high-end tornadogenesis for all 208 supercells. The RFD occlusion was associated with the RFD surge and typically formed 5 to 10 minutes prior to the tornado. Analysis showed that the tornado formed well inside the RFD for 201 of the 208 cases (96.6%), and just inside or along the RFD boundary for seven of the 208 cases (3.4%). Three processes involving the RFD surge were documented. The first setup started with the low-level mesocyclone above the RFD. The RFD's leading edge surged toward the supercell's forward flank. The low-level mesocyclone moved deeper into the RFD, as the RFD occlusion developed under the meso. After this, the tornado formed within the RFD occlusion (66.3%). The second setup started with the low-level mesocyclone ahead of the RFD boundary. The RFD's leading edge surged underneath the low-level mesocyclone, moving toward the forward flank. The low-level mesocyclone moved deeper into the RFD, as the RFD occlusion developed under the meso. After this, the tornado formed in the RFD occlusion (30.3%). The third setup started with the low-level mesocyclone ahead of the RFD boundary. The RFD boundary surged to near the center of the low-level mesocyclone, and the tornado formed in an occlusion along the RFD boundary (3.4%). For most cases relative to the RFD, the RFD occlusion moved in a southwestward direction across the RFD's northeast quadrant.

On average, three cell mergers were documented prior to the tornado. Using the 208 case averages, the first cell merger occurred around 15 minutes prior to the tornado start time and took almost a minute and a half to instigate the RFD surge. The second cell merger occurred about seven minutes prior to the tornado start time, reinforcing the RFD surge, and instigating or aiding development of the descending reflectivity core (DRC). The third cell merger occurred about two and a half minutes prior to the tornado start time, helping to strengthen rotational velocity within the RFD occlusion just prior to the tornado. The study resulted in the following hypothesis. The role of the RFD surge is to push the RFD boundary toward the forward flank downdraft boundary, concentrating an inflow channel between the two boundaries. In response, inflow wind speeds into the supercell dramatically increase, strengthening the low-level mesocyclone. A pressure drop occurs across the inflow channel as it forms, which deepens the surface low associated with the RFD occlusion. The RFD surge pushes the supercell's inflow sector away from the intensifying RFD occlusion, reducing the negative effects of vertical shear on the developing axis of vertical vorticity. For the tornado to form, the column of vertical vorticity must be lined up with the low-level mesocyclone, and the mesocyclone must be sufficiently strong.

1. INTRODUCTION

Much work has been done over the last six decades concerning tornadogenesis in supercells. In the latter half of the 20th century and in the early part of the 21st century, numerous studies have been done on tornadogenesis in high-end supercells. Some of those studies include Fujita 1975, Lemon and Doswell 1979, Klemp and Rotunno 1983, Rotunno 1986, Markowski et al. 2002, 2003, Davies-Jones 2006, Lewellen and Lewellen 2007, Marquis et al. 2008, Markowski and Richardson 2009, Lee et al. 2012, Kosiba et al. 2013, Bluestein et al. 2015 and Skinner et al. 2015. Much of the research on tornadogenesis throughout the years has focused on the rear flank downdraft (RFD) as important to tornadogenesis. And storm observations have confirmed this to be true. Additionally, many tornadogenesis studies have focused on cell mergers. Some of the studies on cell mergers with tornadic supercells include Lee et al. 2006, Wurman et al. 2007, Rogers and Weiss 2008, Rogers 2012, Kurdzo et al. 2015, Tanamachi et al. 2015 and Flournoy 2022.

Parts 1 to 3 of this project, aim to expand our understanding of tornadogenesis through detailed observational analysis. Our main goal has been to learn more how the various supercell features contribute to the formation of high-end tornadoes, in frequency, timing and causation. This paper (Part 1) focuses on the results for the RFD surge, RFD occlusion and cell mergers. Part 2 covers the descending reflectivity core (DRC), inflow channel and streamwise vorticity current (SVC).

2. METHODOLOGY

In order to put together the puzzle pieces of high-end tornadogenesis, we determined that a relatively large sample of supercells with high-end tornadoes would be needed. High-resolution radar would be analyzed for measuring as many characteristics of these supercells as possible. An archive of WSR-88D high-resolution radar, at the Storm Prediction Center, would be used to satisfy most requirements for data collection. Other data, including surface observations and soundings, would be used to analyze environmental information. It was determined that about a decade of radar data would be sufficient for the needs of this project. The period in the archive from May 22, 2008 to December 31, 2019 was examined. Before a tornado event was added to the study, seven criteria must be met (listed below).

1) A supercell mesocyclone must be present in velocity data. The mesocyclone was identified on the lowest elevation angle using storm relative velocity, unless otherwise stated.
2) A forward flank must exist, distinguishing it from a bow echo. Forward flanks were evident with storms that had a mesocyclone.
3) The lowest elevation cut through the low-level mesocyclone must be at 8,000 feet or less.
4) An RFD occlusion, associated with tornado development, must not be preceded by another RFD occlusion within the previous 5 minutes.
5) At least one volume scan without an RFD occlusion, must be present between RFD occlusions.
6) A one-minute gap must exist between the tornado being analyzed and the end of the previous tornado.
7) High-resolution radar must be available for storms more than 50 nautical miles from the radar. High-resolution radar was used for 20 of the 26 storms on April 27, 2011. Low-resolution radar was used for six on that day, all within 50 nautical miles of the radar.

After these criteria were applied to each case, a database was established consisting of 208 supercells associated with EF3 to EF5 tornadoes. The dates and times of each tornado were entered onto a spreadsheet using the Storm Events Database. For one case, the tornado start time was adjusted five minutes earlier, based on a debris ball and 91 knot gate-to-gate shear.

3. RFD OCCLUSION

Although radar analysis can be subjective depending upon the method used, a large database can decrease the effects of subjectivity by sheer volume. The first step of the analysis was to examine the RFD occlusion for all 208 supercells and determine the start and end times.

The method to identify the start and maturation times of the RFD occlusion is listed below.

1) An inflow notch develops north of the potential RFD occlusion area.
2) Reflectivity angle at the inflection point, where the RFD and FFD boundaries converge, decreases to less than 90 degrees.
3) Curvature is exhibited along the leading edge of RFD precipitation.

The inflection point is a place along the southern edge of the supercell on the southwest flank, where the RFD and FFD boundaries converge. It is usually prominent in a supercell before the tornado begins. We used reflectivity thresholds of 35 and 50 DBZ to identify the inflection point. Before the RFD occludes, the angle of the precipitation gradient near the inflection point is greater than 90 degrees. When this angle decreases to less than 90 degrees, it is evident that the RFD is occluding. When this happened, and the inflow notch exceeded 0.4 nautical miles in width with a radar estimated elevation at or below 8,000 feet, we recorded the time as the start of the RFD occlusion process. This time was the first indication that an RFD surge was taking place.

During the analysis, a certain radar signature was common at the start of the RFD occlusion process. This signature became more evident as the RFD occlusion organized, until a peak in organization was reached. This signature was called the pre-tornadic RFD occlusion signature, of which four examples are shown in Figure 1. The four cases averaged about 5 minutes prior to the tornado start time.

RFD Occlusion Signature in Four High-end Supercells

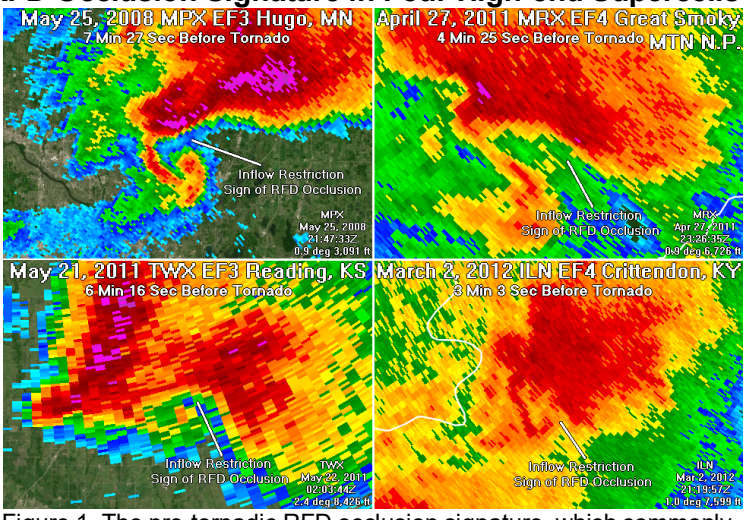

Figure 1. The pre-tornadic RFD occlusion signature, which commonly occurred about five minutes prior to the tornado start time. This signature is an indication that the RFD occlusion has matured and occurs about two-thirds of the way through tornadogenesis.

After the start time of the RFD occlusion was recorded, all scans between that time and the tornado start time were analyzed to determine when the pre-tornadic RFD occlusion signature maximized. The best RFD occlusion signature was identified, and the time of that reflectivity scan was recorded as the end time of the RFD occlusion process.

After the examination was finished, an RFD occlusion had been identified for each of the 208 supercells, just prior to the EF3 to EF5 tornado.

To explore the variance of this process in all cases examined, the results of the RFD occlusion analysis were divided into two parts. A division was made between west and east of the Mississippi River. The average start and maturation times are shown for each region in Table 1. According to the analysis, the RFD occlusion process begins about 10 minutes prior to the tornado start time and ends as the RFD occlusion matures, at just under 5 minutes prior to the tornado start time.

Table 1. RFD Occlusion Times Relative To Tornado Start Time

	Min / Sec Prior To Tornado Start Time		
RFD Occlusion	Start Time	Maturation Time	Duration
102 Cases East of MS River	10:22	4:42	5:40
106 Cases West of MS River	10:17	4:32	5:45
208 Case Average	10:19	4:37	5:42

Average times were remarkably similar east of and west of the Mississippi River. Despite case-to-case differences, the sample is large enough to reveal similar mean characteristics when divided geographically. These results also confirm Robert Davies Jones' declaration that the RFD occlusion process occurs 5 to 10 minutes prior to the start of the tornado (Davies-Jones 2006).

While we do acknowledge that some error remains in the analysis, we have tried to minimize that error by devising robust repeatable identification techniques. The RFD occlusion results showed consistency across events, and established confidence in our method of analysis.

After analyzing the RFD occlusion, each storm was examined in detail to identify as many characteristics as possible for the 208 high-end tornadic supercells.

By the end of the project, the total amount of time to analyze the 208 supercells was about 1,500 hours. The following seven categories were considered the most important for each supercell, although much more data was collected.

1) RFD Surge Type, RFD Surge Start and End Times
2) Tornado Start Location Relative To RFD Boundary
3) Descending Reflectivity Core Type and Location
4) Cell Merger Start Times Relative to RFD Surge and Tornado Start Times
5) Inflow Connection Time Relative to Tornado Start Time
6) Inflow Channel Start and End Time
7) RFD Speed and Direction Relative To The Supercell's Speed and Direction

Figure 2 shows the features of a supercell and is a modification of a schematic from Lemon and Doswell 1979. The graphic is for a supercell at the violent tornado stage, with the positions shown for the RFD (red), FFD (blue), updraft (brown) and tornado (purple). In Figure 3, the tornadic storm that produced a long track EF3 at Salyersville, Kentucky is shown for comparison, with positions drawn for the RFD, RFD boundary, FFD, occlusion downdraft, nose of the occlusion downdraft and inflection point.

It is important to differentiate between the rear flank downdraft and forward flank downdraft (FFD) because these two features are quite different. The inflection point is usually prominent in tornadic supercells, except at peak levels of organization.

Supercell Schematic at Violent Tornado Stage

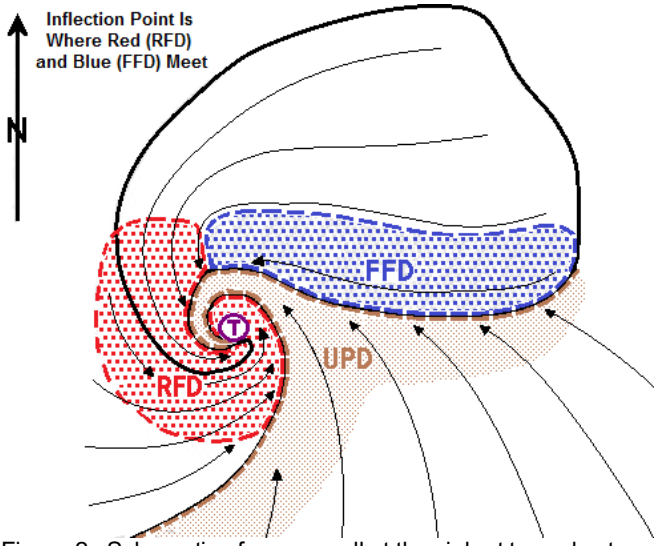

Figure 2. Schematic of a supercell at the violent tornado stage (adapted from Lemon and Doswell 1979). The rear flank downdraft is red, forward flank downdraft is blue, updraft is brown and tornado is purple. The inflow channel is the narrow corridor (brown) north and west of the tornado. The inflection point (blue to red) is located north of the inflow channel. Streamlines are at 300 meters above ground level.

The following four points discuss our hypothesis based on radar observation.

1) The inflection point divides the RFD toward the south from the FFD toward the east. The RFD consists of strong angular momentum and has less access to the supercell's inflow instability. The RFD is associated with less vertical shear and is better able to organize vertical vorticity than the FFD.

2) In contrast to the RFD, the FFD consists of less angular momentum, and has more access to the supercell's inflow instability. Vertical shear is often maximized within the FFD and it is able to organize and maintain horizontal vorticity.

3) As the supercell organizes, the RFD develops a larger-scale rotation oriented in the vertical, while the FFD does not. The FFD can obtain strong rotation within the horizontal plane after the RFD surges and the supercell's forward flank organizes.

4) After the tornado forms, the inflection point can remain intact until peak organization is reached. This advanced state of organization is rare and generally occurs with high-end tornadic supercells near maximum tornado strength. At that time, the FFD boundary gets pulled around by the precipitation gradient along the eastern edge of the hook. The RFD and FFD remain in a similar location, but the inflection point gets washed out as the inflow channel reaches a peak level.

Figure 4 shows six notable high-end tornadic supercells, all at a peak organization. Each supercell has the inflection point washed out with an extremely well-organized inflow channel. This is a sign of a high-end tornado.

4. RFD BOUNDARY

A method was also created to find the location of the leading edge of the RFD, which consists of a prominent boundary. To execute this method, the lowest elevation reflectivity scan closest to the tornado start time was found for each storm, along with the corresponding base velocity and storm relative velocity scans. The reflectivity scan nearest to each tornado averaged 18 seconds before the base velocity scan. These images were analyzed to estimate the position of the RFD boundary. The reflectivity and base velocity scans were used

High-end Supercell at Salyersville, KY (Mar 2, 2012)

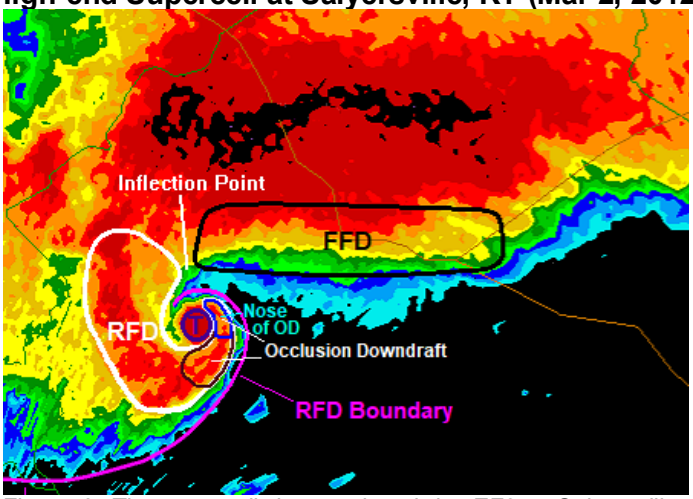

Figure 3. The supercell that produced the EF3 at Salyersville, Kentucky on March 2, 2012. The RFD boundary is purple and occlusion downdraft is encircled in maroon just southeast of the tornado. The nose of the occlusion downdraft is circled in blue just east-northeast of the tornado. Davies-Jones 2006, Markowski 2002, Lee et al. 2011, 2012 explain more about the occlusion downdraft.

RFD/FFD Boundary Locations For Six Well-organized High-end Supercells

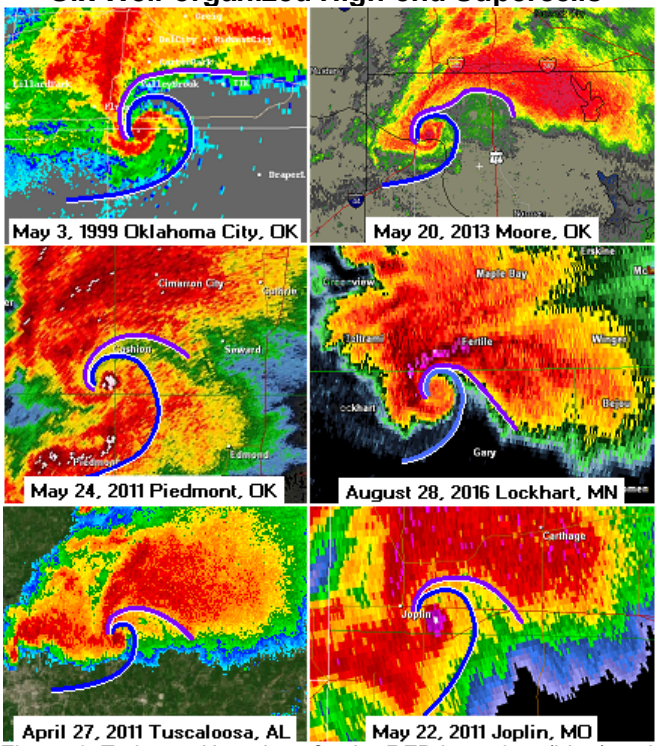

Figure 4. Estimated locations for the RFD boundary (blue) and FFD boundary (purple) for six notable high-end tornadic supercells. These supercells were at peak organization with the inflection point washed out.

together to identify the most likely location of the RFD boundary. Initially, both the reflectivity and base velocity scans were examined. A determination was made on whether the RFD boundary was more evident on the reflectivity scan or the base velocity scan. Often, the base velocity scan did not show the RFD boundary well because winds gradually veered along the boundary lacking an abrupt wind shift. Overall, reflectivity was more effective at identifying the most likely location of the RFD boundary. Often, the RFD boundary could be identified by the presence of increasing reflectivity, notably just to the west of the boundary. In cases where the RFD boundary did not show up on reflectivity near the low-level mesocyclone, it could often be identified further south

and southwest. From there, the boundary could be estimated by drawing a gradually curving arc to the supercell's inflection point. After the reflectivity or base velocity scan was chosen as best for the RFD boundary position estimate, the estimated boundary location was marked on the image along the edge of each bin representing the location with the highest probability of occurrence. The reflectivity scan was used to draw the estimated location of the RFD boundary for 130 of the 208 cases (62.5%). The base velocity scan was used to draw the estimated location of the RFD boundary for 78 of the 208 cases (37.5%).

In order to plot the distribution of each tornado relative to the estimated RFD boundary location, a line had to be drawn on a transparency to be used as a reference point in order to plot the distribution. To make this RFD boundary line, a best fit line was made using the estimated RFD boundary locations for the first 11 cases. As the analysis for each case was done, the positions of the tornado start location were marked on the transparency relative to this RFD boundary line. The northern extent of the drawn RFD boundary for each case was lined up with the northern point of the curved RFD line, and the eastern most point of the drawn RFD boundary was lined up with the eastern most point of the curved RFD line. In this way, each case was plotted on the transparency, resulting in a distribution of points relative to the RFD boundary.

Examples of RFD boundary estimation, using the earlier described method, are shown in Figure 5, 7 and 8.

Reflectivity Boundary Position Estimate

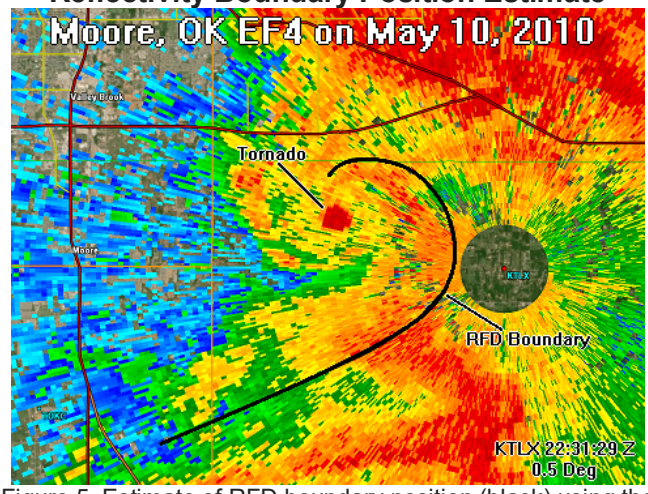

Figure 5. Estimate of RFD boundary position (black) using the reflectivity image for Moore, Oklahoma on May 10, 2010. For every RFD boundary estimate, both reflectivity and base velocity were used together, but one was chosen as primary.

Figure 5 has the RFD boundary marked on reflectivity, while Figure 7 and 8 have it marked on base velocity to the right, and on reflectivity to the left. For that example as in all cases, both reflectivity and base velocity were used for the RFD boundary estimate. In Figure 7 and 8, base velocity showed the RFD boundary best. The RFD boundary position was first drawn on base velocity and then transposed to reflectivity.

When the velocity scans had the best indication of the RFD boundary location, base velocity was more accurate than storm relative velocity (SRV). This is because the RFD boundary moves along the ground, and it is better to estimate the position using a ground-relative approach.

To better understand the position estimates, a schematic of the classic RFD is shown in Figure 6 from Markowski et al. 2002. The RFD occlusion, and then the tornado, develop within the northeast quadrant of the RFD. This happens a considerable distance away from the supercell's inflow sector in most cases. Over the years, many schematics of supercells have been drawn. Some have suggested that the tornado develops in the supercell's inflow region between the RFD and FFD boundaries. However, the Markowski et al. 2002 graphic matches well to our radar analysis, with the tornado developing inside the northeast quadrant of the RFD, a considerable distance to the south-southeast of where the RFD and FFD boundaries converge. For the high-end tornadoes we analyzed, this was most often the case.

Schematic of a Classic Rear Flank Downdraft

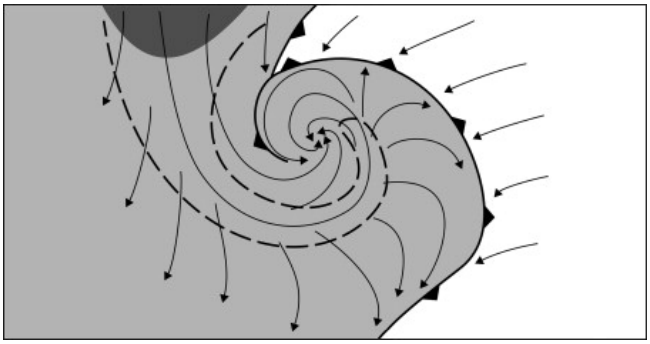

Figure 6. A schematic showing the rear flank downdraft of a tornadic supercell. The RFD occlusion or tornado is at the center of rotational convergence within the RFD. The curved dashed line is the outline of the hook echo. The white area is inflow to the updraft. Gray indicates relatively warm downdraft outflow. An unstable RFD is favorable for tornadogenesis. A couple hundred meters above the surface, winds generally turn south-southwest or southwesterly in the area south of the hook. Graphic obtained from Markowski et al. 2002.

Base Velocity Estimate Overlaid on Reflectivity Base Velocity RFD Boundary Position Estimate

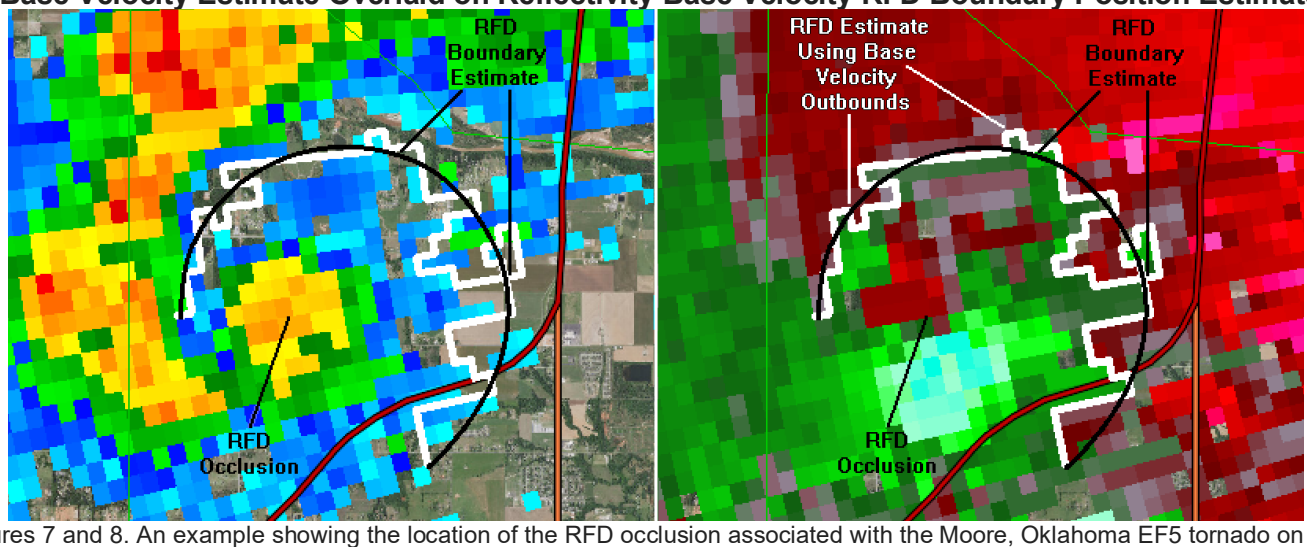

Figures 7 and 8. An example showing the location of the RFD occlusion associated with the Moore, Oklahoma EF5 tornado on May 20, 2013. Base velocity (right) was used as primary to draw the RFD boundary. This location in black was super-imposed onto reflectivity (left). Even though base velocity was the primary indicator for the estimate, reflectivity also shows the RFD boundary well.

Estimated Tornado Start Location Relative To RFD Boundary Position For 208 Cases

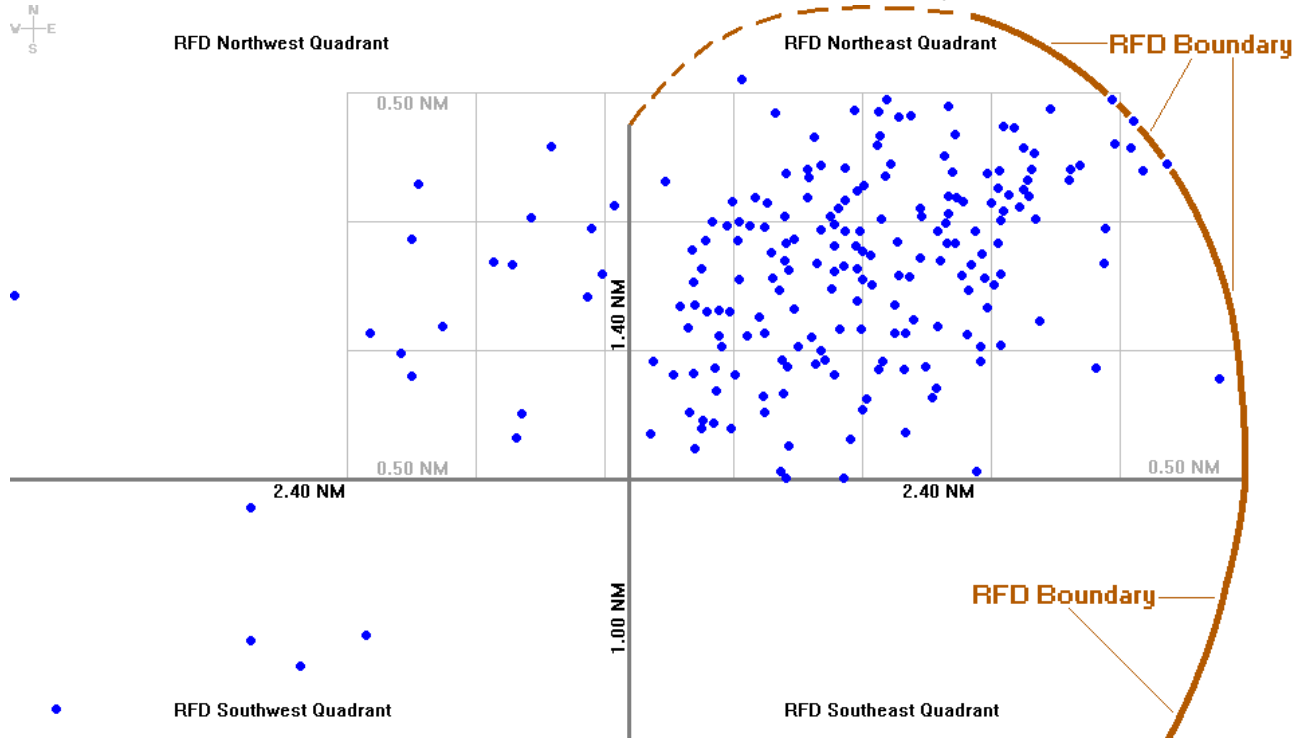

Figure 9. The distribution of tornadoes relative to the RFD boundary near the tornado start time. 201 of the 208 tornado start locations (96.6%) were more than a quarter nautical mile to the west of the RFD boundary. Seven of the 208 cases (3.4%) were located near the RFD boundary, with three of the seven (1.4%) located on the RFD boundary itself.

Figure 9 shows the point distribution of estimated tornado start positions of all 208 supercells relative to the RFD boundary. These positions were found using the reflectivity and base velocity methods shown in Figures 5, 7 and 8. 201 of 208 cases (96.6%) were located well to the west of the RFD boundary, while seven cases (3.4%) were located within one-quarter of a nautical mile of the RFD boundary. Certainty for the RFD boundary estimate was high for 191 of the 208 cases (91.8%). For the 17 low confidence cases (8.2%), all 17 were located more than a quarter mile away from the RFD boundary. Of the seven cases within a quarter nautical mile of the RFD boundary, three were inside the RFD just to the west of the RFD boundary, three appeared to be located on the RFD boundary itself, and one was located well to the south-southeast just inside the RFD boundary. For the 208 cases, no tornado was found to have started to the east or north of the RFD boundary. The inflow channel was found to be north of the RFD, wrapping cyclonically around the RFD's northern edge, and the streamwise vorticity current (SVC) was found to straddle the inflow channel and forward flank downdraft. These two features will be covered in Part 2 of this study. Figure 9 suggests that most EF3 to EF5 tornadoes form in the northeast quadrant of the RFD, and that the RFD is important to tornado formation.

Tornado Start Location Frequency Relative To RFD Boundary Position For 208 Cases

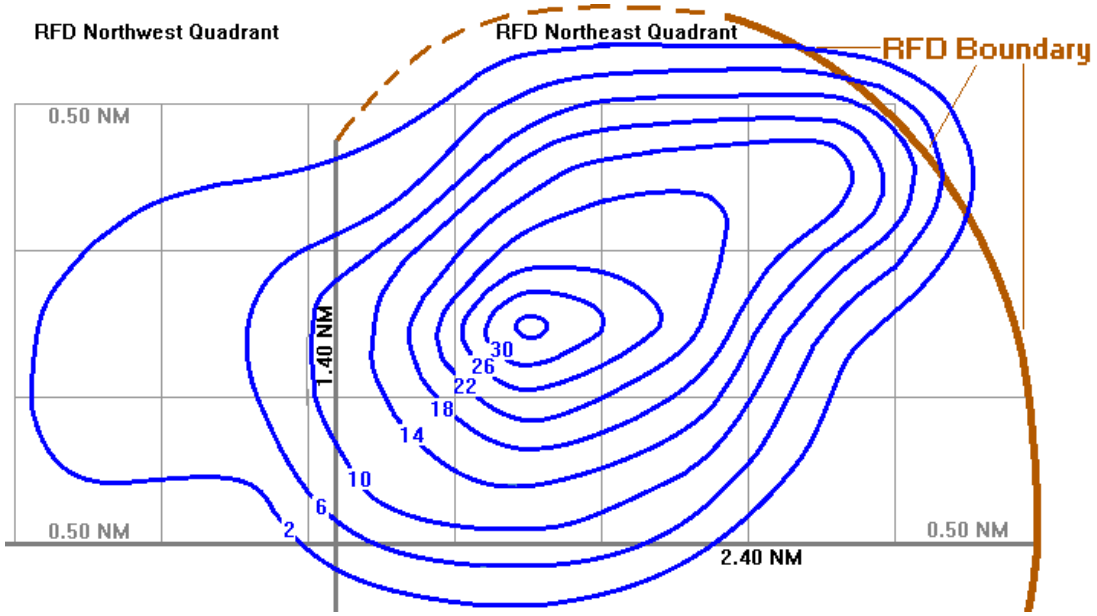

Figure 10. Contoured estimate of tornado start location relative to the position of the RFD boundary for 208 high-end tornadic supercells. The highest tornado incidence occurred 1.65 nautical miles west and 1.07 nautical miles south of the RFD boundary.

Figure 10 shows the contoured distribution of tornado start location relative to the position of the RFD boundary. On average, the most frequent tornado start location was 1.65 nautical miles to the west of the RFD boundary and 1.07 nautical miles to the south of the RFD boundary. An axis of higher incidence is located from near the RFD boundary extending southwestward across the northeastern quadrant of the RFD.

Figure 11 shows the distribution of tornado start location relative to the RFD boundary, divided up into six components. The left column shows the distribution for the first half and second half of the dataset. The second period from May 22, 2008 to March 2, 2012 (lower left) has a more concentrated distribution compared to the first period from March 15, 2012 to December 16, 2019 (upper left). This is likely due to the high number of large tornado outbreaks during the second period. On the plot (lower left), April 27, 2011 (26), March 2, 2012 (9), May 24, 2011 (6) and April 10, 2009 (5) were responsible for 46 (44.2 %) of the tornadoes. Thus, the environments were more similar in this period of the dataset.

The two graphics in Figure 11 (middle), divide the distribution between east and west of the Mississippi River. The three cases along the RFD boundary occurred to the west of the Mississippi River (lower middle), otherwise the distributions are very similar. The two graphics in the right column of Figure 11 show the distribution when the leading indicator for the RFD boundary estimate was reflectivity (upper right), and when the leading indicator for the RFD boundary estimate was base velocity (lower right).

Figure 12 and 13 show the EF4-EF5 tornado start location distribution (left), and EF5 tornado start location distribution (right), relative to the RFD boundary. On average, violent tornadoes most often form deep within the northeast quadrant of the RFD.

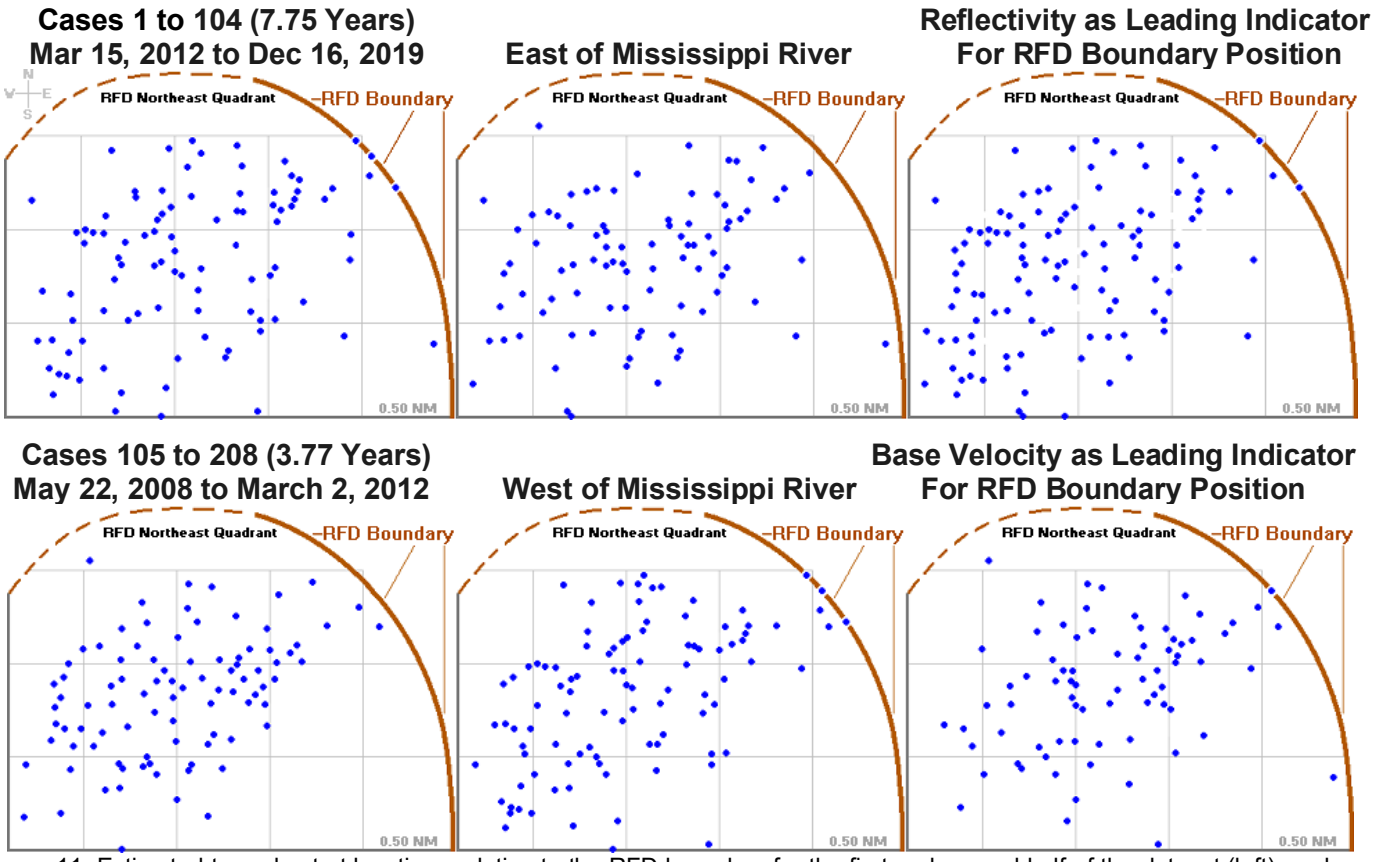

Figure 11. Estimated tornado start locations relative to the RFD boundary for the first and second half of the dataset (left), and east and west of the Mississippi River (middle). The distribution of points is shown for the reflectivity and base velocity scans (right), depending upon which one was used as the primary indicator.

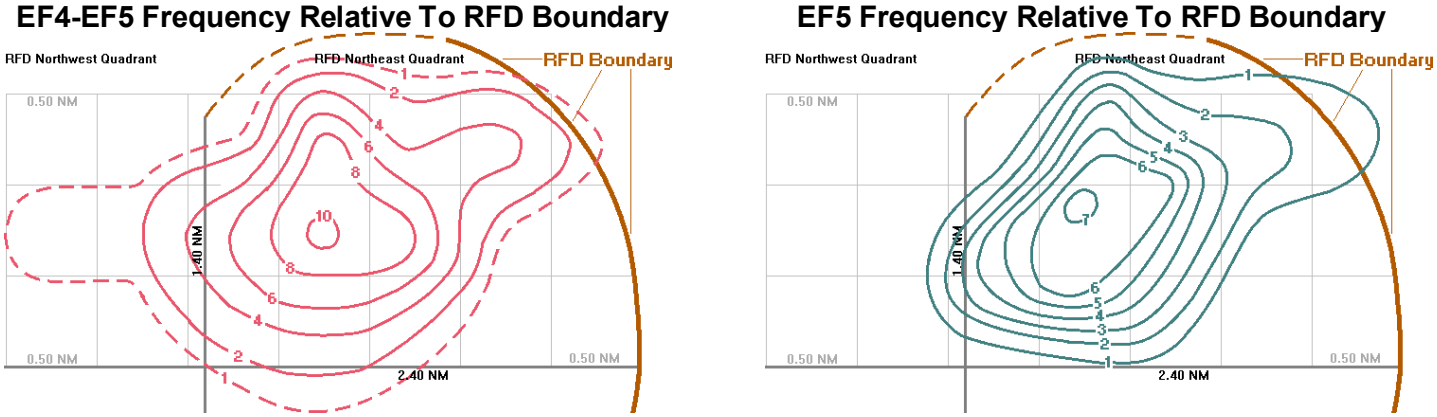

Figures 12 and 13. Frequency of EF4-EF5 tornadoes (left) and EF5 tornadoes (right), relative to the position of the RFD boundary.

5. RFD SURGE

One objective of this study was to identify processes that were common to all high-end tornadic supercells. We found this to be true of the RFD surge. The RFD surge consistently occurred during tornadogenesis and was one of the easier features to analyze. There is no doubt complexity within the RFD surge, as was documented by Skinner et al. 2014. In Part 1 of this study, we have identified a primary RFD surge that seems to be consistent across events. A secondary RFD surge occurs internally and is associated with the DRC (covered in Part 2). The DRC is a distinct downdraft core within or near to the pendant or hook of a supercell that usually drops gradually to the surface in strong flow and more quickly in weaker flow.

During the analysis, the RFD surge appeared to be an important part of tornadogenesis. Figure 14 depicts three sectors of the supercell, including the forward flank downdraft (red), rear flank downdraft (blue) and inflow sector (green). The RFD boundary, at the RFD's leading edge, is black. On average for the 208 cases, the RFD surge starts just over 13 minutes before the tornado begins. The RFD surge creates the inflow channel as the RFD boundary impinges the inflow sector. On average, the inflow channel starts around 5 minutes before the tornado start time, coinciding with SVC formation (covered in Part 2).

The RFD surge could be characterized by two components. The first involves a downdraft that remains located within a similar location in the supercell and generates a strong outflow that moves away from the area. This outflow can accelerate as it moves horizontally along the ground. The second component involves precipitation that is developing and moving more quickly than the supercell. Air along the edges of this developing downdraft is forced to move horizontally along the ground away from the precipitation core. In most cases, these two components work together to support the RFD surge.

For high-end tornadogenesis, radar analysis from this study suggests that the RFD surge is a response to enhanced outflow, almost always associated with cell mergers (see section 6). Increased low-level rotation contributes to the RFD surge depending upon how close the RFD surge is to the low-level mesocyclone. But most often the cell merger, along with upscaled convective growth associated with the cell merger, appears to be the main contributor. The RFD surge can begin a considerable distance away from the low-level mesocyclone and often appears to be an independent process. The outflow just ahead of the cell merger can also contribute to the RFD surge. A sudden increase in the low to mid-level flow associated with a jet streak, can also strengthen and sustain the RFD surge, as is covered in Part 3 of this study.

Schematic Created and Modified After The First 50 Storms Were Analyzed Showing the RFD Surge, Inflow Channel Formation and Tornado Development on a Temporal Scale

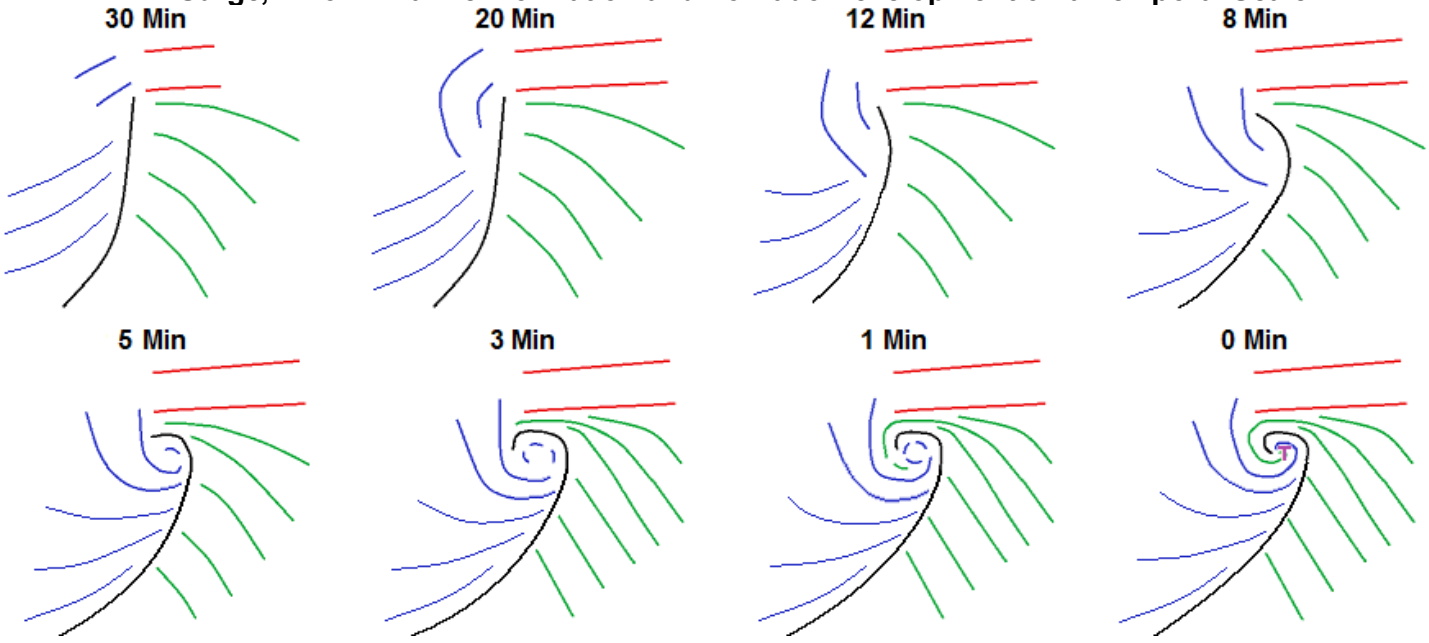

Figure 14. A schematic showing the process of tornadogenesis involving an RFD surge beginning just over 13 minutes before the tornado start time. The RFD surge creates the inflow channel, as the RFD surge impinges on the inflow sector. This likely induces a pressure drop due to the Bernoulli Effect, which strengthens the RFD occlusion. The tornado forms after the RFD occlusion matures beneath the low-level mesocyclone, most often in the RFD's northeast quadrant.

Figure 15 shows a sequence of events that occurred in tornadogenesis for numerous cases. The following description is a key hypothesis of this study. First, the RFD surge pushes underneath the low-level mesocyclone (far left). At that time, the RFD occlusion develops just behind the RFD boundary. As the RFD boundary pushes towards the forward flank, the RFD occlusion deepens and matures beneath the mesocyclone (middle). The RFD occlusion appears to move southwestward relative to the RFD, as the RFD boundary moves further away towards the northeast.

As the RFD boundary approaches the FFD boundary, an inflow channel is created (right in Figure 15). Measurements during the analysis showed that winds approximately doubled within the inflow channel. This can be explained by the Bernoulli Effect which induces a pressure drop across the inflow channel. This pressure drop is likely enhanced as air is evacuated upward through the mesocyclone at a faster rate than can be replaced below. In response, the RFD occlusion rapidly deepens. The tornado forms after the RFD occlusion matures. This hypothesis will be covered in greater detail after the RFD analysis section.

Schematic of RFD Surging Beneath Mesocyclone with Rapid Intensification of RFD Occlusion Due To Restriction From Developing Inflow Channel

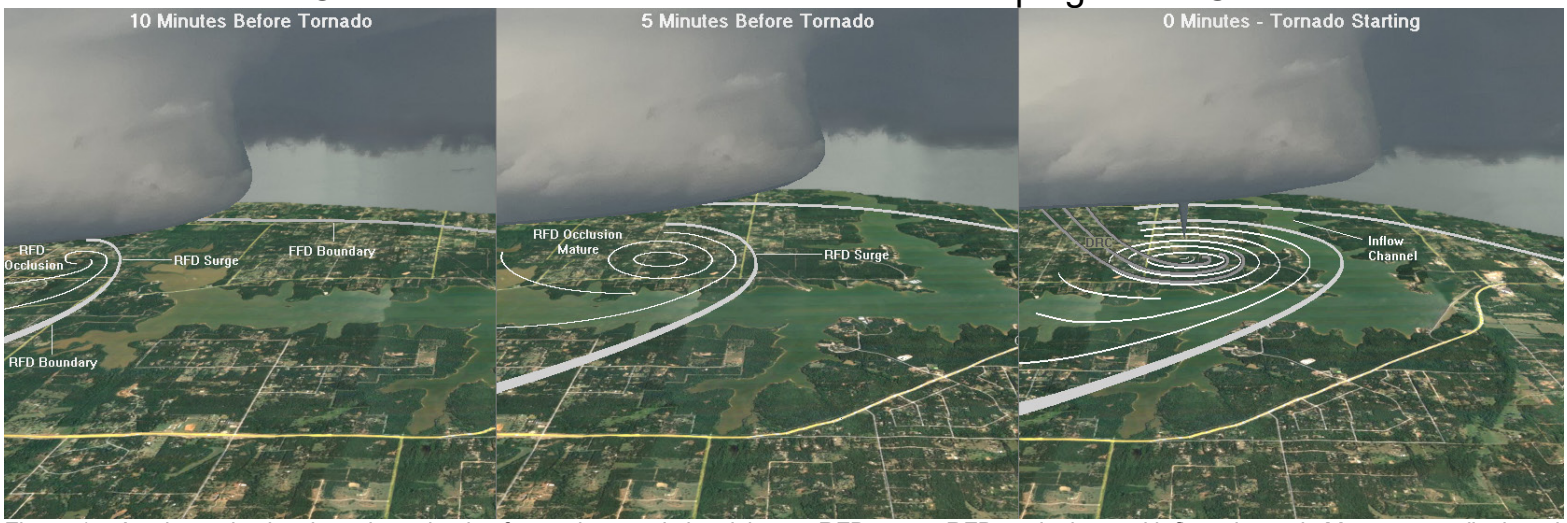

Figure 15. A schematic showing a hypothesis of tornadogenesis involving an RFD surge, RFD occlusion and inflow channel. Many cases displayed a similar sequence, with the RFD occlusion developing just behind the RFD boundary, and then moving southwestward relative to the RFD. This happens because the RFD boundary surges northeastward toward the forward flank. As the RFD boundary impinges on the supercell's inflow sector, an inflow channel is created. This induces a pressure drop due to the Bernoulli Effect, which strengthens the RFD occlusion. Also, restriction within the inflow channel causes the RFD occlusion to rapidly deepen as air is evacuated upward through the mesocyclone at a faster rate than can be replaced below. The tornado forms after the RFD occlusion matures beneath the low-level meso, most often in the RFD's northeast quadrant. The descending reflectivity core (DRC) is in dark gray, which wraps around the RFD occlusion near the tornado start time (see Part 2).

RFD SURGE ANALYSIS

An RFD surge was found for all 208 cases. The following method was used to identify the start and end points of the RFD surge, and to measure the RFD surge's speed relative to the supercell's speed.

First, the case was loaded and studied for about 15 minutes. The tornado start location was marked. Then, the RFD boundary location was estimated at high confidence times before and after the tornado start time. The examination paid close attention to the movement of precipitation behind the RFD boundary. Four questions listed below, were asked in order to determine when the RFD surge started and ended.

1) When did the precipitation gradient, just behind the RFD boundary, begin to accelerate relative to the storm's movement?
2) When did the precipitation gradient, just behind the RFD boundary, obtain a bowed or curved appearance?
3) When did the precipitation gradient, just behind the RFD boundary, reach the forward flank?
4) When did the precipitation gradient, just behind the RFD boundary, decelerate relative to the storm's movement?

Reflectivity data were used exclusively to determine when the RFD surge began and ended. The RFD surge was considered a time period when the leading edge of precipitation, just behind the RFD boundary, moved at a speed faster than the supercell's speed. This involved an acceleration and then deceleration of the leading edge of precipitation.

After becoming strongly familiar with the case, a point representing the RFD surge start location, was marked along the precipitation gradient's leading edge, usually either at 35 DBZ or 50 DBZ. Using the chosen DBZ level, the leading point of the surge was manually tracked over the series of reflectivity scans during the RFD surge. This was done to achieve time continuity. On the last scan of the RFD surge, an ending point was marked at the same DBZ threshold used for the starting point. In addition to the same DBZ threshold, the starting and ending points were sought to have a similar distance ratio along the length of the precipitation gradient. For example, if the starting point on the first scan was a quarter of the distance along the leading edge of precipitation, an ending point was selected on the last scan, a quarter of the distance along the leading edge of the precipitation gradient.

Every effort was made to achieve case-to-case consistency. Once the start and end locations of the RFD surge were identified, the series of reflectivity scans between the two points was rechecked to make sure that the start and end points appeared to be strongly representative.

After the initial analysis was done, the case was reexamined later. If there was some uncertainty in the original analysis, then the same method was done to obtain a second set of points. If two sets of points were identified, then the set of points that seemed to best represent the RFD surge was used. If both sets of points were deemed representative, the higher speed of the two was used. If uncertainty still existed, analysis on the case could be stopped, and picked up at a later time. Priority was placed on obtaining a set of points for each case that was accurate and representative. This tedious task took a substantial amount of scrutiny and time.

Once a representative set of points was obtained, the speed of the supercell was measured using reflectivity scans approximately 15 minutes before and 15 minutes after the tornado start time. At both times, the inflection point was found at either 35 DBZ or 50 DBZ. The distance that the inflection point traveled was measured between the two scans. This distance and the time differences between the inflection point's starting and ending points with matching DBZ, were used to determine the supercell's speed. Then, the supercell's speed was subtracted from the RFD surge speed, to obtain the RFD surge's storm relative speed.

Figure 16 shows the RFD surge analysis for the Sibley, Iowa EF4 tornado on June 25, 2010. A cell merger ongoing in panel 1, initiates the RFD surge at 17 minutes 33 seconds prior to the tornado start time. The RFD surge starting point is highlighted in panel 2, at the southern corner of a relatively straight corridor of precipitation at 35 DBZ. This point was chosen as the RFD surge starting point because it was the last time that the precipitation corridor was bulge free. In most cases, the precipitation corridor in the form of a pendant, will begin to show curvature just after the RFD surge begins. For this case, the initial bulge is evident in panel 3.

RFD Surge Analysis - Sibley, IA EF4 June 25, 2010

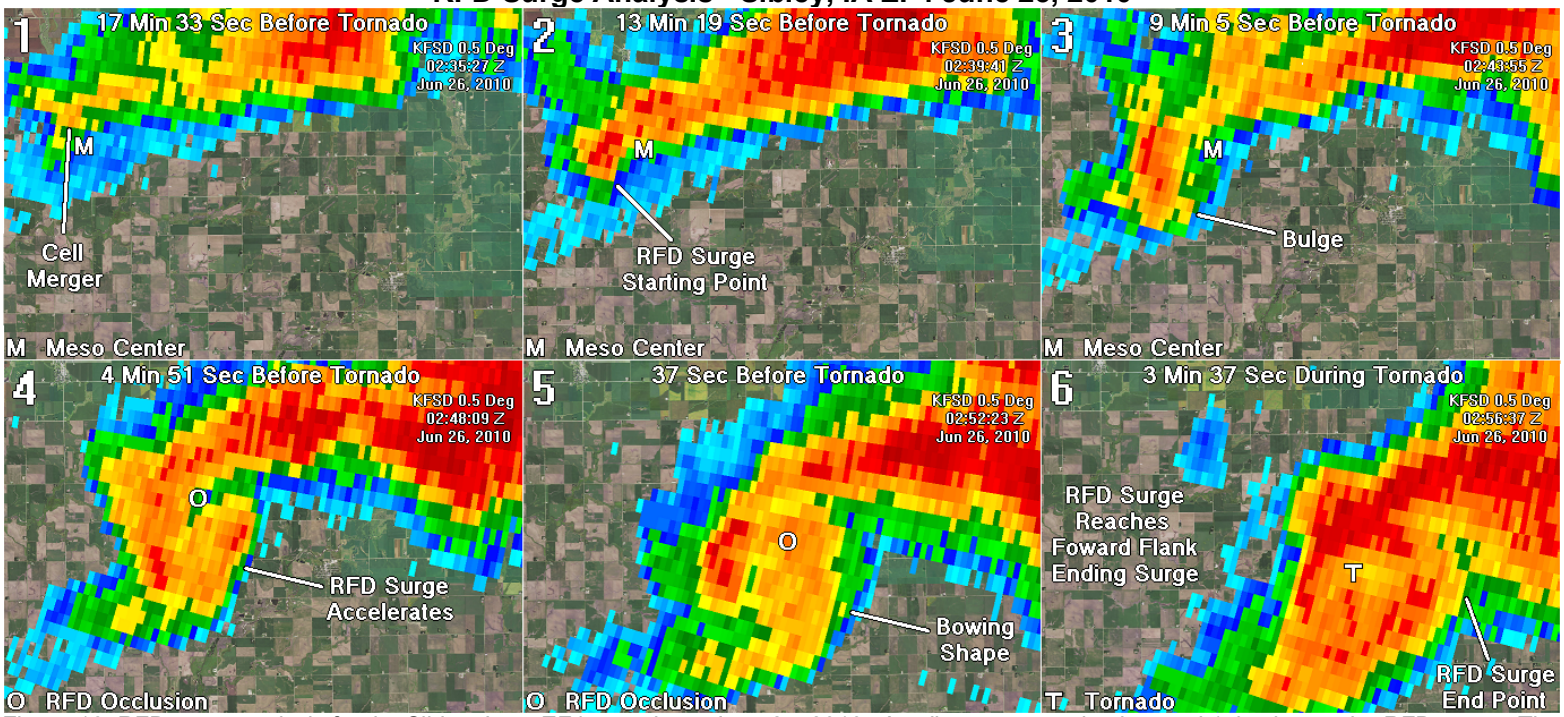

Figure 16. RFD surge analysis for the Sibley, Iowa EF4 tornado on June 25, 2010. A cell merger ongoing in panel 1, instigates the RFD surge. The RFD surge starting point (panel 2) and ending point (panel 6), are marked. During the RFD surge, the reflectivity structure bulges and rapidly expands (panel 3 and 4). A bowing shape develops in panel 5. The RFD surge ends when it reaches the forward flank (panel 6).

Reflectivity rapidly expands as the RFD accelerates eastward in panel 4. A bowing shape develops along and behind the RFD boundary in panel 5. The RFD occlusion, denoted by the "O", forms well behind the leading edge of the RFD in panel 4 and 5. The tornado begins in panel 6, and the RFD surge ends when the RFD's leading edge reaches the forward flank.

For this case, the RFD surge lasted 16 minutes 56 seconds and traveled at 7.9 nautical miles per hour relative to the supercell. Both of these are close to the 208 case average.

Figure 17 shows a distribution of all 208 cases with the RFD surge's storm relative speed. The 208 case average had the RFD surge moving 6.9 knots faster than the speed of the supercell. RFD surge speeds, relative to the supercell's speed, varied from just under two nautical miles per hour to just over 20 nautical miles per hour. The distribution for RFD surges in the 208 case database is relatively smooth, which increased confidence in the RFD surge analysis. Approximately one-third of the cases had a surge less than 5.0 nautical miles per hour relative to the supercell's speed. This showed that a fast RFD surge speed is not necessary for tornadogenesis. As is hypothesized by this study, the role of the RFD surge is to reduce the distance between the RFD and FFD boundaries. This creates an inflow channel, which markedly strengthens inflow within it, and helps deepen the surface low in the RFD. This further strengthens the RFD occlusion and intensifies the low-level mesocyclone, just prior to the tornado.

Three types of RFD surges were identified, shown on the next two pages. The first type in Figure 18, occurred for 138 of the 208 cases (66.3%). This type involves a setup in which the low-level mesocyclone is initially located vertically above the RFD. The RFD boundary surges toward the forward flank, as the low-level meso moves southwestward relative to the RFD. The RFD occlusion develops and matures under the low-level mesocyclone. The tornado develops within the RFD occlusion, most often in the RFD's northeast quadrant.

The second type in Figure 19, occurred for 63 of the 208 cases (30.3%). This type involves a setup in which the low-level

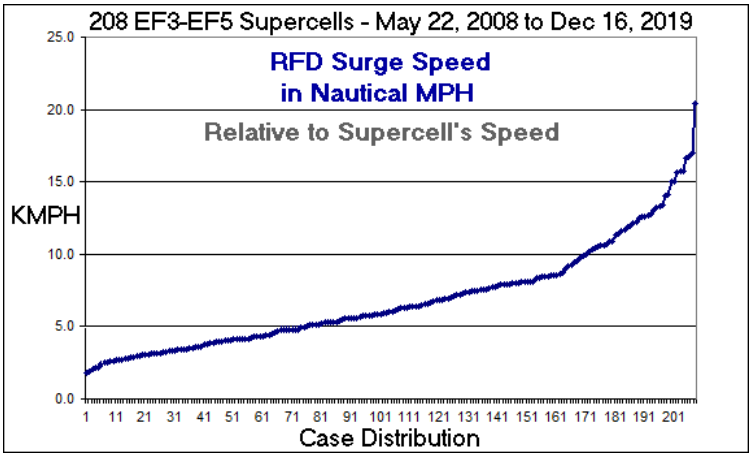

Figure 17. Sorted distribution of RFD surge storm relative speed for all 208 supercells. The average RFD surge storm relative speed ranged from just under two knots to just over 20 knots. The RFD's primary role during tornadogenesis is to move the RFD boundary toward the FFD boundary, in order to create an inflow channel. A fast storm relative speed is not necessary to accomplish this task.

mesocyclone is initially ahead of the RFD boundary. The RFD's leading edge surges beneath the low-level mesocyclone and then pushes toward the forward flank. The RFD occlusion develops and matures after the RFD surge has undercut the low-level mesocyclone. The tornado forms within the RFD occlusion, most often in the RFD's northeast quadrant.

The third type in Figure 20, occurred for seven of the 208 cases (3.4%). This type involves a setup in which the low-level mesocyclone is initially ahead of the RFD boundary. The RFD boundary surges toward the supercell's forward flank, reaching the center of the low-level mesocyclone. An RFD occlusion forms on the RFD boundary under the low-level mesocyclone. The tornado forms within the RFD occlusion on the RFD boundary, before moving southwestward into the RFD.

RFD Surge Type 1 (66.3%) Rozel, KS EF4 - 5/19/2013

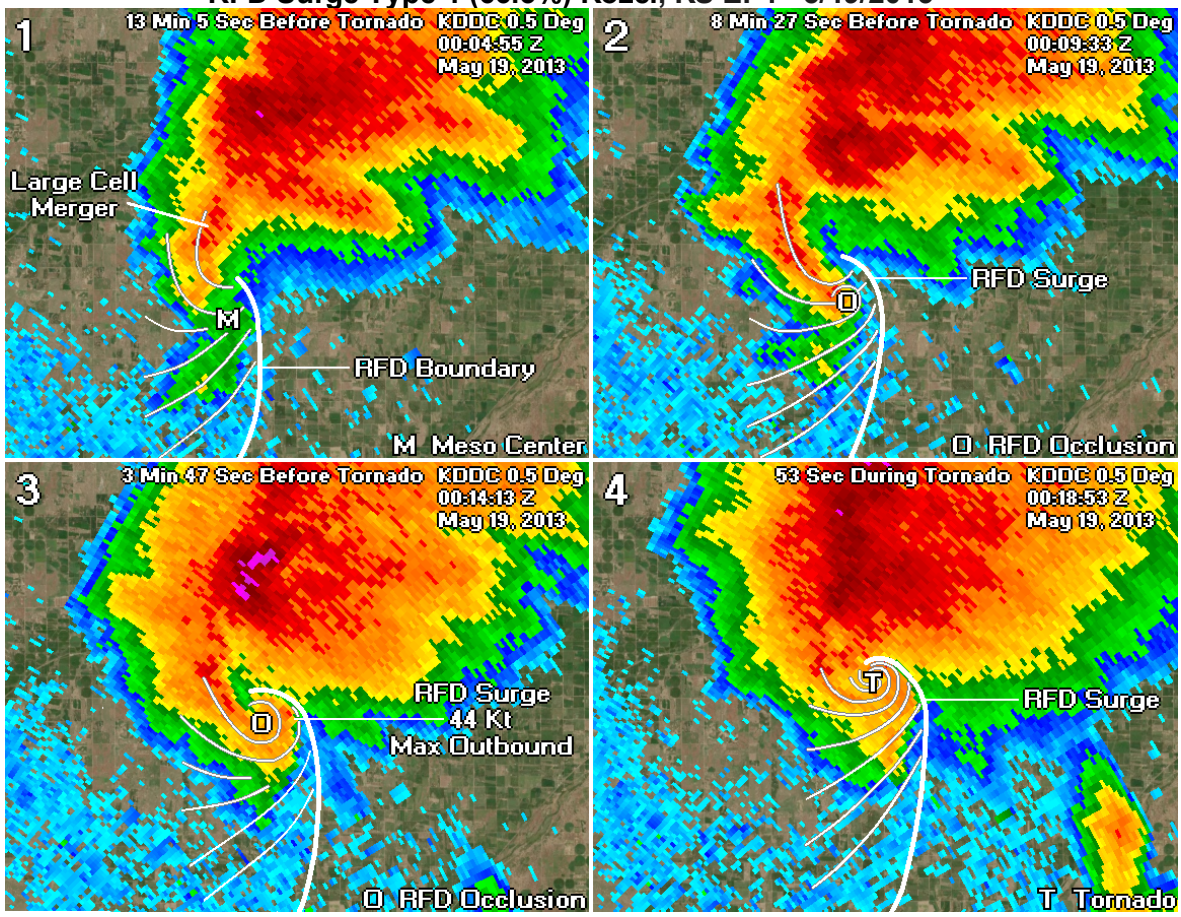

Figure 18. Type 1 RFD surge (at right), in which the low-level mesocyclone is initially above the RFD. During the RFD surge, the RFD boundary moves toward the supercell's forward flank. The RFD occlusion develops and matures, which is followed by tornado formation in the RFD occlusion. The tornado most often forms in the northeast quadrant of the RFD.

For the Rozel, Kansas EF4 tornado on May 19, 2013 (at right), a prominent cell merger started the RFD surge. The mesocyclone was located to the west of the RFD boundary (panel 1). The cell merger caused an enhanced downdraft to move southeast, creating a long pendant (panel 2). The RFD occlusion developed at the pendant's southeast end. The tornado formed as the RFD boundary surged northeastward toward the forward flank. This created a narrow inflow channel (panel 3 and 4). 300 meter ground-relative flow is estimated based on cell movement and outflow.

RFD Surge Type 2 (30.3%) Fackler, AL EF4 - 4/27/2011

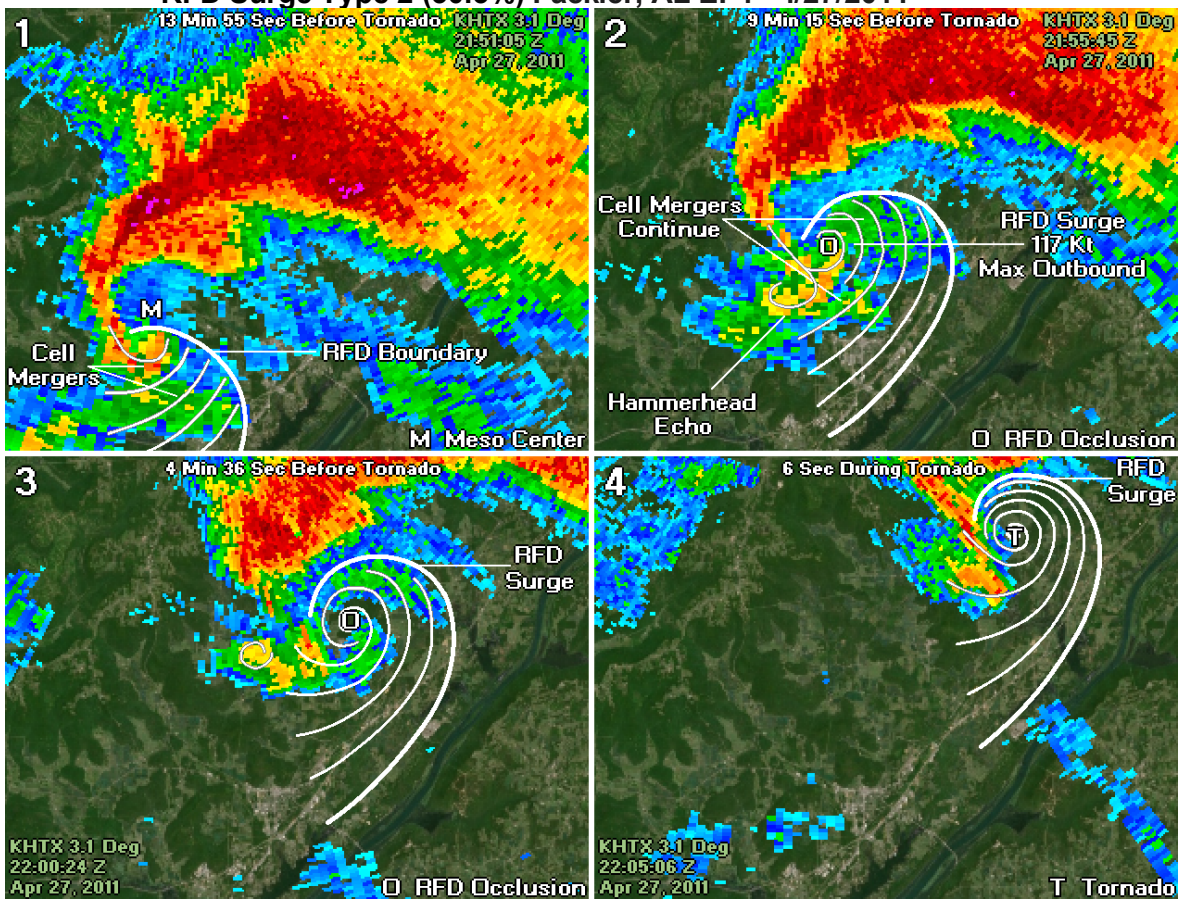

Figure 19. Type 2 RFD surge (at right), in which the RFD surge is initially ahead of the RFD boundary. The RFD boundary moves underneath the low-level mesocyclone and then away toward the forward flank. The RFD occlusion develops and matures after the low-level mesocyclone has been undercut. This is followed by tornado formation within the RFD occlusion.

For the Fackler, Alabama EF4 tornado on April 27, 2011 (to right), the RFD surge was instigated by cell mergers to the southwest of the RFD boundary. The RFD surge was very strong, with a 117 knot max outbound noted in panel two. The inflow channel became narrow as the RFD boundary pushed toward the forward flank (panel 3). Reflectors quickly disappear around the new tornado (panel 4), likely due to absorption by the rapidly strengthening tornado. 300 meter ground-relative flow is estimated based on cell movement and outflow.

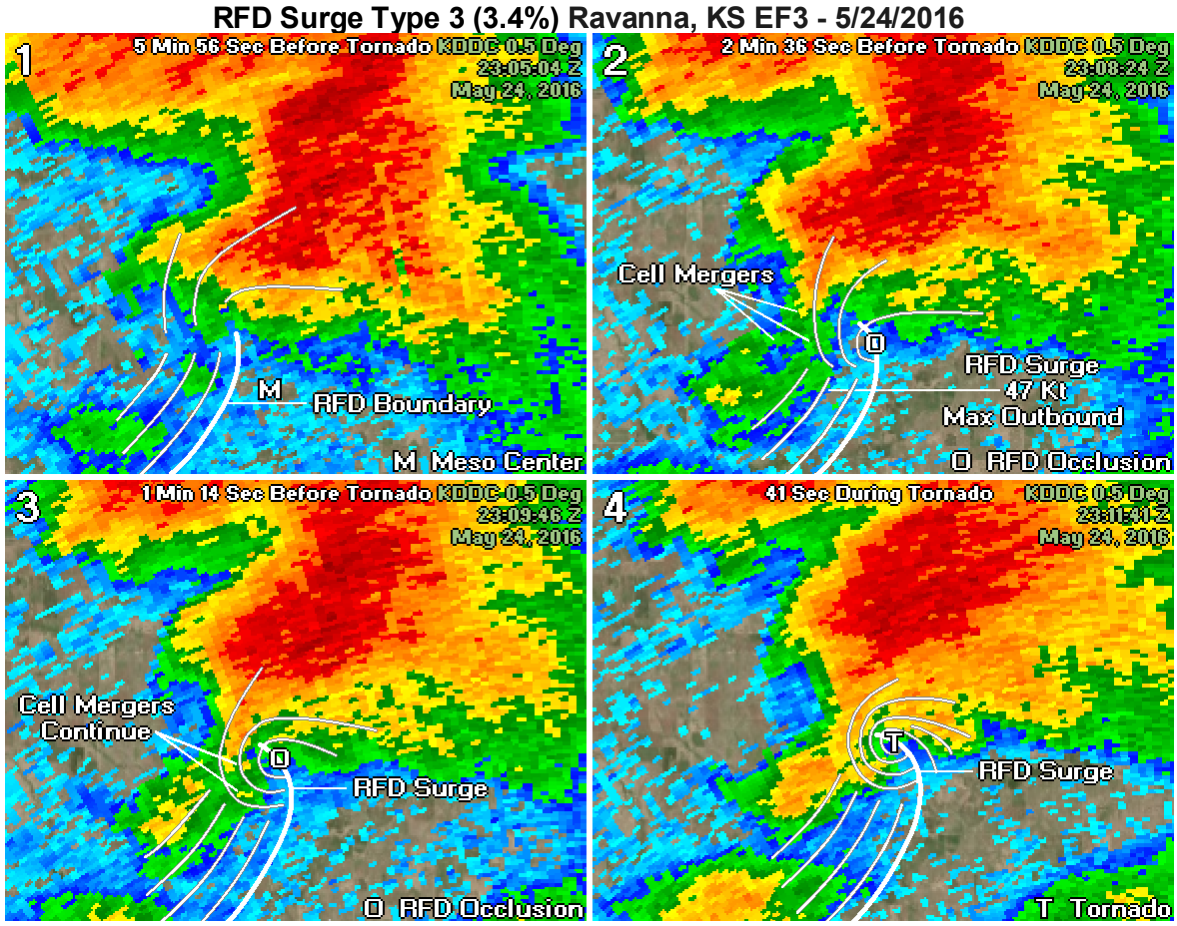

Figure 20. Type 3 RFD surge (at right), in which the low-level mesocyclone is initially ahead of the RFD boundary. The RFD boundary surges toward the supercell's forward flank, and to the center of the low-level mesocyclone. An RFD occlusion forms on the RFD boundary, underneath the low-level mesocyclone. The tornado develops within the RFD occlusion, on the RFD boundary, eventually moving southwestward into the RFD.

For the Ravanna, Kansas EF3 tornado on May 24, 2016 (at right), the mesocyclone was initially to the east of the RFD boundary. The RFD surge was instigated by outflow associated with cell mergers west of the boundary (panel 2). As the RFD surged toward the forward flank, the RFD occlusion developed on the RFD boundary (panel 2 and 3). Then, the tornado formed in the RFD occlusion (panel 4). 300 meter ground-relative flow is estimated based on cell movement and outflow.

Average start and end times were calculated for all 208 cases. On average, the RFD surge began over 13 minutes prior to the tornado start time and ended just over 4 minutes after the tornado start time. On average, the RFD surge duration was just under 18 minutes, traveling 12 nautical miles. On average for the 208 cases, the RFD surge moved at 40.9 nautical miles per hour relative to the ground from 245.5 degrees.

Average RFD Surge Times Relative To Tornado Start Time For All 208 Supercells

RFD Surge Start Time	13 Min 31 Sec Before
RFD Surge End Time	4 Min 21 Sec After
RFD Surge Duration	17 Min 53 Sec

The RFD surge appears to be critical to tornadogenesis in these cases for the two reasons listed below, related to this study's hypothesis.

1) The RFD surge pushes the inflow sector of the supercell back as the RFD boundary approaches the forward flank. The inflow channel forms when the RFD boundary moves toward the FFD boundary, creating a narrow corridor between the two boundaries. A pressure drop occurs across the inflow channel due to the Bernoulli Effect (detailed in Part 2). Radar estimates show that when air enters the inflow channel, wind speeds approximately double. As the inflow channel narrows, the pressure continues to drop, and winds strengthen more. When this happens, air is evacuated upward through the updraft faster than inflow air can enter into it from below, which amplifies the pressure drop across the entire RFD. This rapidly deepens the surface low associated with the RFD occlusion, which intensifies near-surface rotation. The strengthened inflow also rises into the updraft and intensifies the low-level mesocyclone (Wicker and Wilhelmson 1995, Marquis et al. 2008).

2) As the RFD surges beneath the low-level mesocyclone, the meso center is displaced deeper within the RFD. As a result, the low-level mesocyclone gains proximity to the descending reflectivity core (DRC), which develops in response to cell mergers along the south-southwestern part of the supercell's pendant (detailed in Part 2). The DRC helps a column of vertical vorticity to organize and protects this column from being sheared apart by low-level vertical shear. Inflow air with low-swirl ratio is partially blocked due to the RFD surge (Lewellen and Lewellen 2007). This results in increased downward motion adjacent to the developing column of vertical vorticity, strengthening rotation at the surface. These factors make conditions favorable for tornado formation.

Vertical shear is necessary to create a strong updraft (Peters et al. 2019) and to intensify the low-level mesocyclone. Horizontal vorticity tilted into the vertical, is the source of rotation for the low-level mesocyclone and ultimately the tornado (P. Markowski 2019 personal communication). However, it is vertical vorticity near ground-level, created along the northern edge of the DRC that is critical to strengthening the circulation just before the tornado forms. If this surface-based vorticity develops underneath the center of the low-level mesocyclone and the low-level mesocyclone is strong enough, a tornado is likely to form.

Early in the project, Jana Houser was contacted at Ohio University to help clarify tornadogenesis. She states,

"The source of vorticity for the low-level meso appears to be the classic horizontal vorticity generated baroclinically along/near the forward flank boundary (I hesitate to call it a 'gust front', but the same idea). That vorticity is generated relatively low in the storm (a few 100 meters or so above the ground) gets advected rearward in a storm relative sense, is tilted upward by the storm's primary updraft, and contributes to strengthening or generating the low-level meso. However, there is a separate source of vorticity that appears to be necessary for tornado formation, and this vorticity is oriented in the vertical plane and is present very near and perhaps adjacent to the surface (heights less than 100 meters). It appears to be relatively shallow in some cases, although in others it is a bit deeper, spanning a few hundred meters. The big question right now is what is the source for this vorticity? Some people argue that this is an extension of the horizontal baroclinic vorticity generation that has been tilted downward by the RFD or within the vertical velocity gradient between

the RFD and the updraft. Other studies have found that it is frictionally generated. It is my personal feeling that there is not one unique way that this near surface vertical vorticity develops, but that there are perhaps several different mechanisms/processes that can potentially do this. What appears to be most important ultimately for tornadogenesis is not so much the formation mechanism behind the vorticity, but the spaciotemporal positioning of this vorticity with the low-level meso. It appears that to get a tornado to successfully develop, the low-level meso must be 'sufficiently strong' to stretch the near ground vertical vorticity upwards and to strengthen it to reach tornadic intensity. This requires the low-level meso to be strong (obviously!), the near ground vertical vorticity to be present, and the two to be physically located in approximately the same place in the storm such that the low-level meso is physically above the near ground vorticity. If something is missing in this 'recipe' tornadogenesis fails."

There is one thing to add to this explanation of tornadogenesis. To get near surface vertical vorticity to be lined up with the low-level mesocyclone, it is critical that the RFD undercut the low-level mesocyclone. The RFD is a favorable area for the generation of vertical vorticity because vertical shear is generally less in the RFD than on the inflow side of the supercell. Although strong vertical shear is critical for the mesocyclone, wind shear can destroy vertical vorticity. This is what prevents hurricanes from forming, and is what happens in tornadolysis, described in detail in Davies-Jones et al. 2001. Our estimates in this study show that 205 of the 208 EF3 to EF5 tornadoes (98.6%) formed inside the RFD, with the other three on the RFD boundary itself. If the low-level mesocyclone is centered on the supercell's inflow side, tornadogenesis at the high-end is very unlikely.

Two cases further illustrate this concept. In Figure 21, the first case is the tornadic storm that produced an EF4 tornado to the southwest of Goldsby, Oklahoma on May 24, 2011. For this case, the EF4 tornado first developed 23 nautical miles southwest of Goldsby. During the hour before the tornado, a left-moving supercell developed in north Texas and moved quickly north-northeastward toward the Goldsby storm at approximately 65 nautical miles per hour. The left-moving storm approached the Goldsby storm and merged with the forward flank while the tornado was ongoing (panel two). Near the cell merger time, the tornado strengthened and reached maximum strength with a VROT of 94.7 knots. Five minutes later, the northward-moving wave, likely associated with strongly backed flow, hit the RFD (panel three). This wave was evident near the Goldsby supercell, but also in low reflectivity data further east. The wave pushed the back edge of the RFD northward away from the tornado (panel four to six). This caused a gradual disruption of the RFD, resulting in a gradual drop in VROT. Fifteen minutes after peak intensity, the tornado started to markedly weaken, as the RFD began to be seriously disrupted. The RFD precipitation then began a steady northward shift (panel seven and eight), causing the tornado to rapidly dissipate, and sparing Norman a direct hit.

Northward-moving Wave Disrupts RFD and EF4 Tornado near Goldsby, OK on May 24, 2011

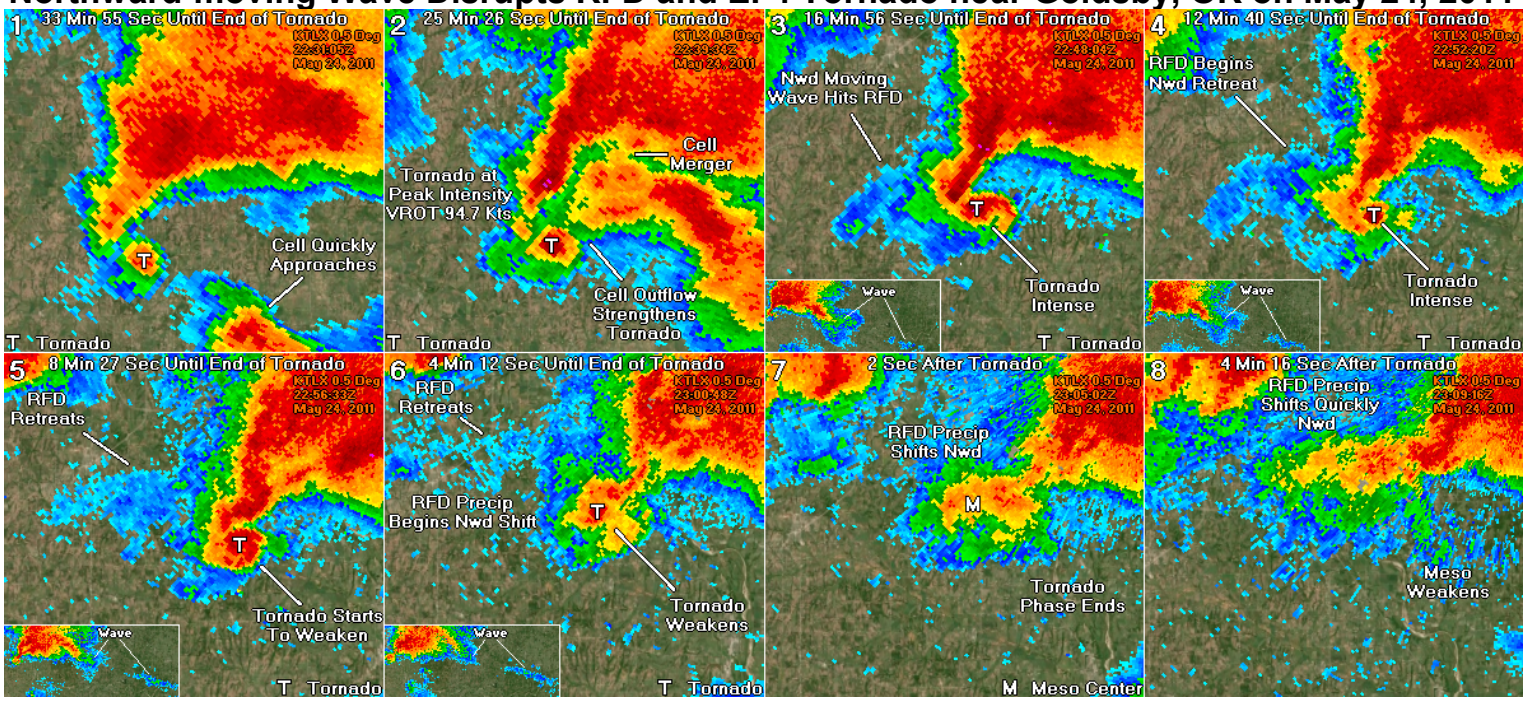

Figure 21. An example showing the Goldsby, Oklahoma EF4 tornado on May 24, 2011, in which the RFD was disrupted by a northward-moving wave. First, a left-moving supercell from north Texas approached the Goldsby supercell at near 65 nautical miles per hour. Outflow associated with the cell merger enhances vertical vorticity, causing the tornado to strengthen and reach peak intensity (panel 2). After the cell merger, a northward-moving wave associated with the left-mover, hit the Goldsby supercell's RFD. The back edge of the RFD retreated northward (panels 4, 5 and 6), and eventually the backed flow associated with the northward-moving wave pushed the flanking line precipitation away from the mesocyclone (panels 7 and 8). This disrupted the RFD causing the tornado to dissipate.

In Figure 22, the second case is the tornadic storm that produced an EF3 tornado at Hillsboro, North Dakota on August 27, 2016. The supercell formed in northwest mid-level flow, moving southeastward across far eastern North Dakota. Two RFD surges preceded the tornado. The first RFD surge (panel one to four) occurred approximately over a 17 minute period, ending at 22:39:50 Z. No tornado was produced during the first RFD surge because it was southwest of the low-level mesocyclone and did not undercut the mesocyclone. Veered northwest mid-level winds, made it difficult for the RFD surge to surge eastward. For this same reason, veered flow makes tornado development less likely. This problem often occurs in summer. The second RFD surge (panel six to ten), occurred approximately over a 22 minute period, ending at 23:03:51Z. During the second RFD surge, outflow associated with a cell merger pushed the RFD surge further east until it undercut the low-level mesocyclone. This occurred, as the RFD occlusion developed eight minutes before the tornado start time (panel eight). The RFD occlusion matured and then the tornado formed in the RFD's northeast quadrant (panel nine and ten). In this case, the RFD surge undercutting the low-level meso, appeared to be the key for tornadogenesis.

EF3 Forms After 2nd RFD Surge Undercuts Low-level Meso at Hillsboro, ND on Aug 27, 2016

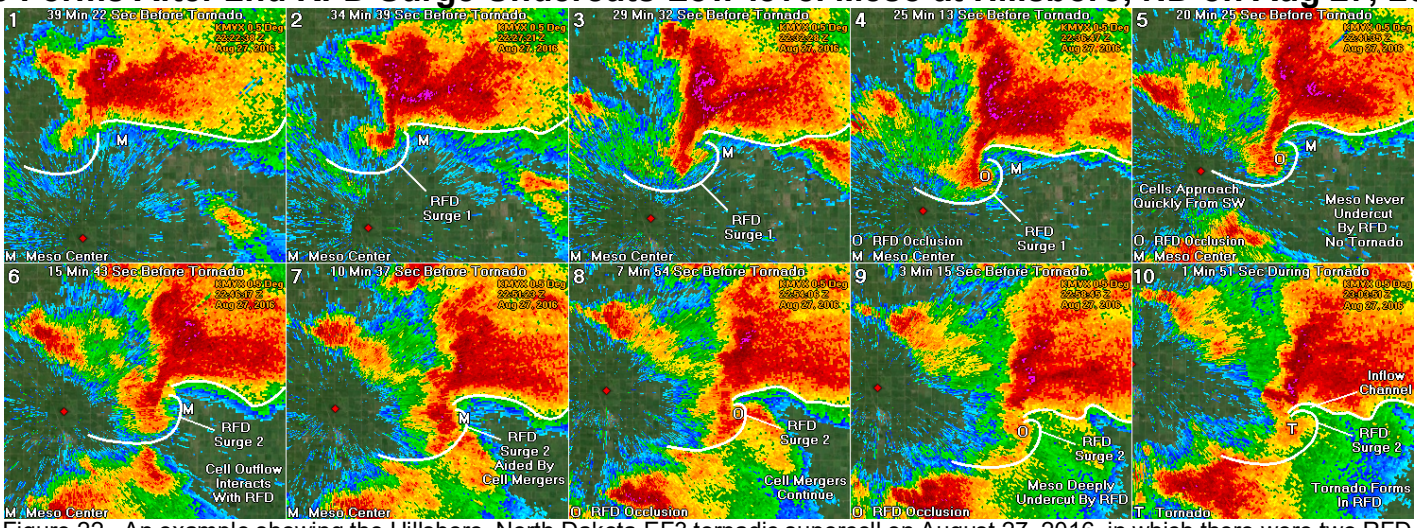

Figure 22. An example showing the Hillsboro, North Dakota EF3 tornadic supercell on August 27, 2016, in which there were two RFD surges. The first RFD surge did not produce a tornado, while the second did. The first RFD surge pushed southward and did not undercut the low-level mesocyclone. Veered flow at 700 mb and a lack of cell mergers were limiting factors, keeping the first RFD surge to the west of the low-level meso. The second RFD surge pushed eastward, undercutting the low-level meso. The second RFD surge was aided by cell outflow and cell mergers during the 15 minutes preceding the tornado. Veered low to mid-level flow, associated with northwest flow aloft, can contribute to a problem in which a supercell's RFD surge takes place too far west. When this happens, it can be difficult for the RFD to undercut the low-level mesocyclone. This problem makes tornadogenesis more unlikely in summer.

6. CELL MERGERS

Cell mergers play a role in tornadogenesis, as several studies have shown, including Bluestein and Weisman 2000, Lee et al. 2006, Wurman et al. 2007, Hastings et al. 2014, and Kurdzo et al. 2015. An updraft rotating aloft is unlikely to produce damage at the surface without a downdraft (Davies-Jones 1982). Cell mergers produce enhanced downdrafts that help tilt vorticity lines downward, helping to intensify the RFD occlusion just prior to tornado formation. The downdraft accelerates as it approaches the ground, potentially helping to drag rotation within the mesocyclone towards the surface. The enhanced downdrafts created by cell mergers can accomplish this important task. Cell mergers have been shown to be associated with increasing rotational velocities for tornadoes of EF2 to EF5 intensity (Rogers 2012).

For analyzing the 208 supercells, a method was created to find the location of cell mergers. To execute the method of identifying a cell merger, a series of reflectivity scans from approximately 30 minutes before the tornado start time to 10 minutes after the tornado start time was examined at the lowest elevation angle. In addition to cell mergers, these images were used to identify the location of descending reflectivity cores (DRCs), covered in Part 2. To identify a cell merger, an individual cell of increased reflectivity was found. The cell must have time continuity and move toward another cell, also with time continuity. There was no low-end qualifying threshold. For a cell merger to be identified, the two cells must move toward one another and collide at their edges. Prior to the cell merger, there must be a difference of greater than 8 DBZ between the maximum DBZ values for the weaker of the two cells and the lowest value between the two cells. The merging cell was considered the fastest moving of the two. For the start of a cell merger to be identified, the DBZ difference between the merging cell's DBZ maximum and the minimum between the two cells must decrease to 8 DBZ or less.

Using the size of each cell and translation speed, an interpolation method was done to estimate the start time of each cell merger. If the cell merger appeared to start just after the scan, then an "early between scans" time was designated. If the cell merger appeared to start just before the scan, then a "late between scan" time was designated. If the cell merger start time was in between scans, but appeared to be neither early or late between scans, then a "midday between scans" time was designated. This interpolation technique increased the cell merger start time resolution to around a minute, with some more recent cases dropping to near a half minute.

The start of a cell merger did not always result in a complete merger. Occasionally, cells temporarily merged, with the merging cell moving past the cell being merged into and the two separating once again. But most often, the two cells appeared to merge completely. This process could occur almost immediately or could take 15 minutes or more. But most cell mergers started and completed within a few minutes. During a cell merger, the outflows of two cells gradually combine which can cause an enhanced maximum in reflectivity. The combined downdraft is stronger than either of the two before the merger, enabling the outflow to spread quickly away from the area. Sometimes, the outflow preceding the merging cell, impacted the cell being merged into just prior to the merger. The effect of an enhanced outflow was similar.

At least one cell merger was found for all 208 supercells. These cell mergers appeared to be important to the RFD surge, development of the DRC or to formation of the tornado. This study's cell merger frequency is much higher than other studies for tornadoes. One explanation is that this study has no lower-end intensity threshold when identifying cell mergers (explained at the left). Other studies have used a strict qualifying intensity threshold. For example, Rogers and Weiss 2008 compiled a five year database of cell mergers, with a lower-bound qualifying threshold of 35 DBZ. We did not use a lower bound threshold for qualification because a lack of precipitation is a poor indictor to determine an absence of downward motion (P. Markowski 2019 personal communication). We have documented many cells of relatively weak intensity, in the 20 to 40 DBZ range, that were likely associated with strong downward motion. And these merging cells likely had an impact on tornadogenesis. Sometimes, the cells were rapidly intensifying when the cell merger occurred. We found other cells that were in this similar intensity range that appeared to be associated with strong outflow. This outflow also likely impacted tornadogenesis. Although all identified cell mergers were documented, cell mergers that appeared to have no impact on tornadogenesis were not included on the distribution graphics or when computing the average times.

In our database, these high-end tornadic supercells were generally associated with several cell mergers, and often three or more. The highest frequency occurred on the south-southwest edge of the pendant or hook. Flournoy et al. 2022 found that supercell low-level mesocyclones generally strengthen when the number of cell mergers increases from one to two, into the three to four range. We also observed this.

During the cell merger analysis, all 208 cases were examined twice. The first examination pass identified cell mergers that occurred closer to the tornado start time. Within this first pass, clustering within the distribution was found at two time periods. The first was found to occur just a few minutes prior to the tornado start time. A second was found further out in time, generally between five and ten minutes prior to the tornado. During the first examination, it was observed that another cell merger was commonly occurring more than 10 minutes prior to the tornado start time. And this cell merger was often happening just before the start of the RFD surge. As a result, a second pass through the 208 cases was completed to identify cell mergers further out before the tornado start time. The cell merger that was identified during the second pass was called cell merger one, while the two cell mergers that were identified during the first pass were called cell merger two and three. After all the analysis was done, a cell merger two was found in more cases than a cell merger one. This is because a cell merger midway through the tornadogenesis process was slightly more common than a cell merger near the beginning of the tornadogenesis process. The first and second examinations were completely independent of each other, which revealed more detail concerning the distribution.

Using the three periods of cell merger clustering, average times prior to the tornado start time were computed. The 208 case average of those times are listed below, with the number of cases identified for each time, and the percent of occurrence listed in Table 1.

Table 1. Times of Cell Mergers Associated with Tornadogenesis Relative to Tornado Start Time

	Time of Occurrence Prior To Tornado Start Time	Cases Identified	Percent of Occurrence
Cell Merger 1	14 min 48 sec	192	92.3%
Cell Merger 2	6 min 54 sec	202	97.1%
Cell Merger 3	2 min 26 sec	132	63.5%

Cell merger one was associated with the instigation of the RFD surge by either the cell merger or outflow just ahead of the merging cell. Cell merger one also instigated the DRC. Cell merger two likely helped reinforce the RFD surge or assisted with vertical vorticity enhancement for the formation of the tornado. Often, it appeared to do both. Cell merger two also helped with development of the DRC, which will be discussed in Part 2. Cell merger three's role appears to assist with vertical vorticity enhancement for tornado formation. Usually, additional cell mergers were observed around the recorded cell mergers. But only cell mergers that were in closest proximity to the RFD surge, RFD occlusion or developing tornado were recorded. To be important to tornadogenesis, the cell merger's resulting outflow must have time to reach the RFD occlusion by the tornado start time. For this determination, careful temporal and spatial analysis was done of the tornadic part of the supercell.

After the cell merger analysis was complete for each storm, the recorded cell merger that instigated the RFD surge was plotted on a transparency showing the pendant drawn as a thick black line. The radar images were zoomed sufficiently such that the outline of the pendant approximately matched the shape and size of the pendant or hook. Then, the position of the cell merger was plotted on the transparency. The resulting plot is shown in Figure 23, with the position of cell merger one relative to the tornado start location. The graphic includes 77 cell mergers that likely instigated RFD surges between June 5, 2010 and March 15, 2012. The most common locations of this type of cell merger occurred from south to southwest of the pendant. One maximum was located to the southwest of the pedant's tip with the other further northwest near the western edge of the pendant.

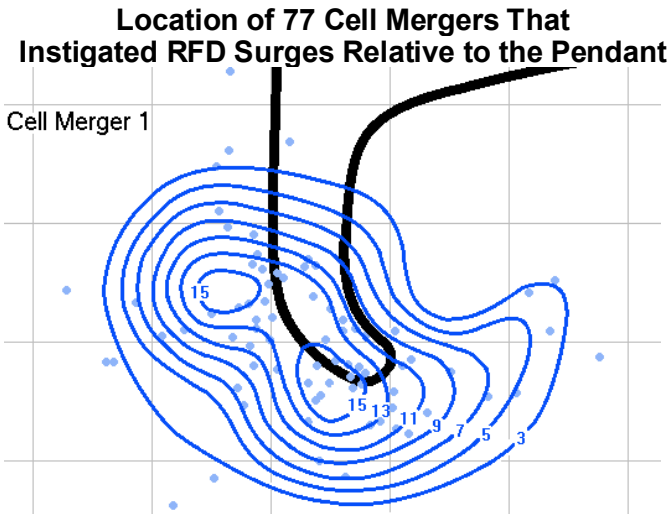

Figure 23. The locations of cell merger one for 77 cell mergers relative to the pendant, that likely instigated RFD surges prior to high-end tornadogenesis from June 5, 2010 to March 15, 2012.

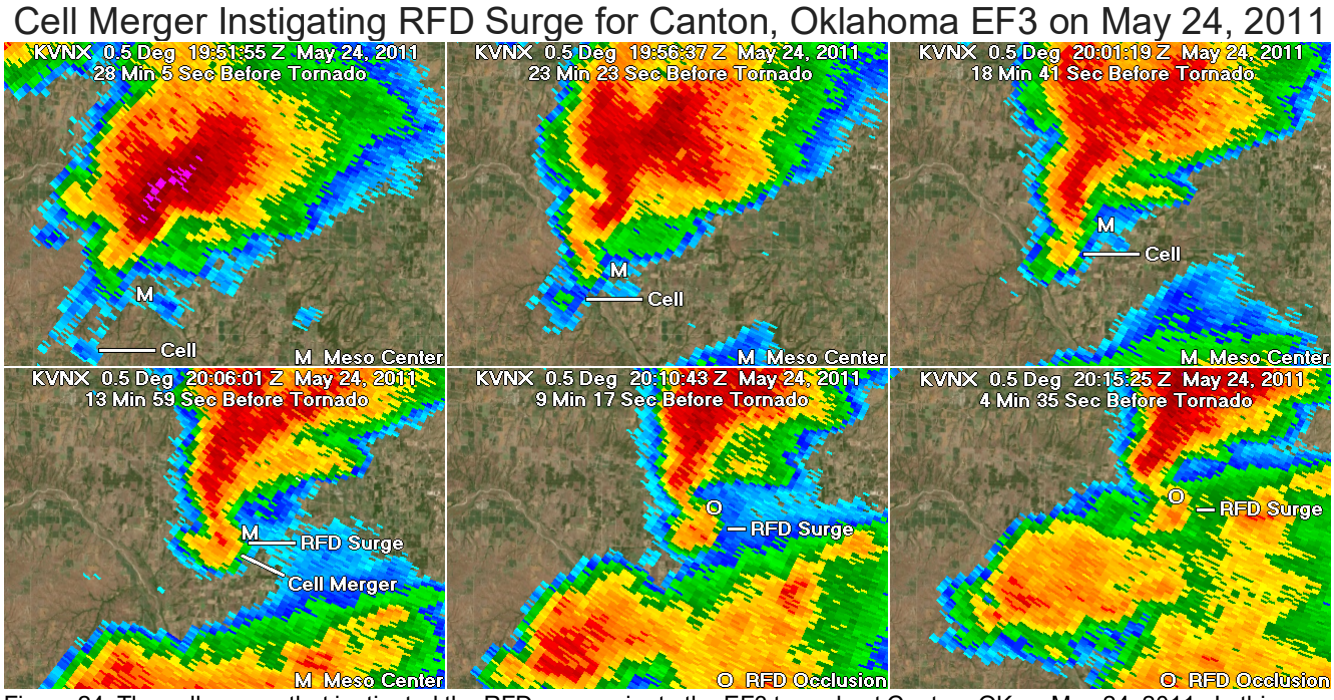

Figure 24. The cell merger that instigated the RFD surge prior to the EF3 tornado at Canton, OK on May 24, 2011. In this case, the merging cell was less than 20 DBZ (upper left and upper middle). But the cell rapidly intensified just before the merger. We found some cases where a weak cell (<= 35 DBZ) was involved with a cell merger likely important to tornadogenesis.

Using the 208 case average, the RFD surge started less than 2 minutes after cell merger one, and over 13 minutes prior to the tornado start time. While low-level rotation around the meso can contribute to the RFD surge, the main contributor appears to be either the enhanced outflow produced by cell merger one, the outflow ahead of cell merger one, or both.

Figure 24 shows a cell merger that appears to instigate the RFD surge prior to the Canton, Oklahoma EF3 tornado on May 24, 2011. The merging cell can be seen as a small area of reflectivity below 20 DBZ in the upper left panel. As the merging cell approaches the supercell's pendant, it increases in intensity. The cell merger occurs with the pendant (lower left panel), resulting in an RFD surge indicated by the curved leading edge of precipitation (lower two right panels). The angle of the RFD and FFD boundaries decreases to less than 90 degrees at that time, providing evidence of the RFD surge, and beginning the RFD occlusion process. The RFD surge's leading edge is denoted by a "reversed C" shape. Often, the RFD surge could be identified when the supercell's pendant became curved in appearance, with the apex of the curve extending in an eastward direction. This case shows how subtle the RFD surge can look on radar. For most other cases, the RFD surge was larger in scale and more pronounced.

Figure 25 shows the RFD surge associated with the Duanesburg, New York EF3 tornado on May 22, 2014. Each panel is centered on the southwestern part of the Duanesburg supercell. This case occurred in northwest mid-level flow and had a storm movement to the south-southeast. In panel 1, a large cell that is likely a severe storm, is located to the northwest of the Duanesburg supercell. The RFD boundary associated with the Duanesburg supercell is relatively straight (panel 1). The large cell further northwest approaches and merges with the back edge of a large pendant extending westward from the Duanesburg supercell's main core, constituting cell merger one (panel 2 and 3). Cell merger one appears to instigate the RFD surge that is evident in panel 4, 5 and 6. Cell merger two has begun in panel 4, which instigates the descending reflectivity core (DRC) and appears to reinforce the RFD surge. The RFD occlusion forms in panel 5 during the height of the RFD surge as the DRC approaches. The tornado forms as the DRC wraps into the circulation in panel 6, just before the end of the RFD surge. Storm-relative trajectories are shown using streamlines based on cell movement and outflow. The DRC is covered extensively in Part 2 of this study.

For the Duanesburg, New York supercell, cell merger two occurred around 10 minutes prior to the tornado start time. This is well before the 208 case average, which had cell merger two starting about seven minutes prior to the tornado start time. But as a whole, the sequence of events shows the method of tornadogenesis well.

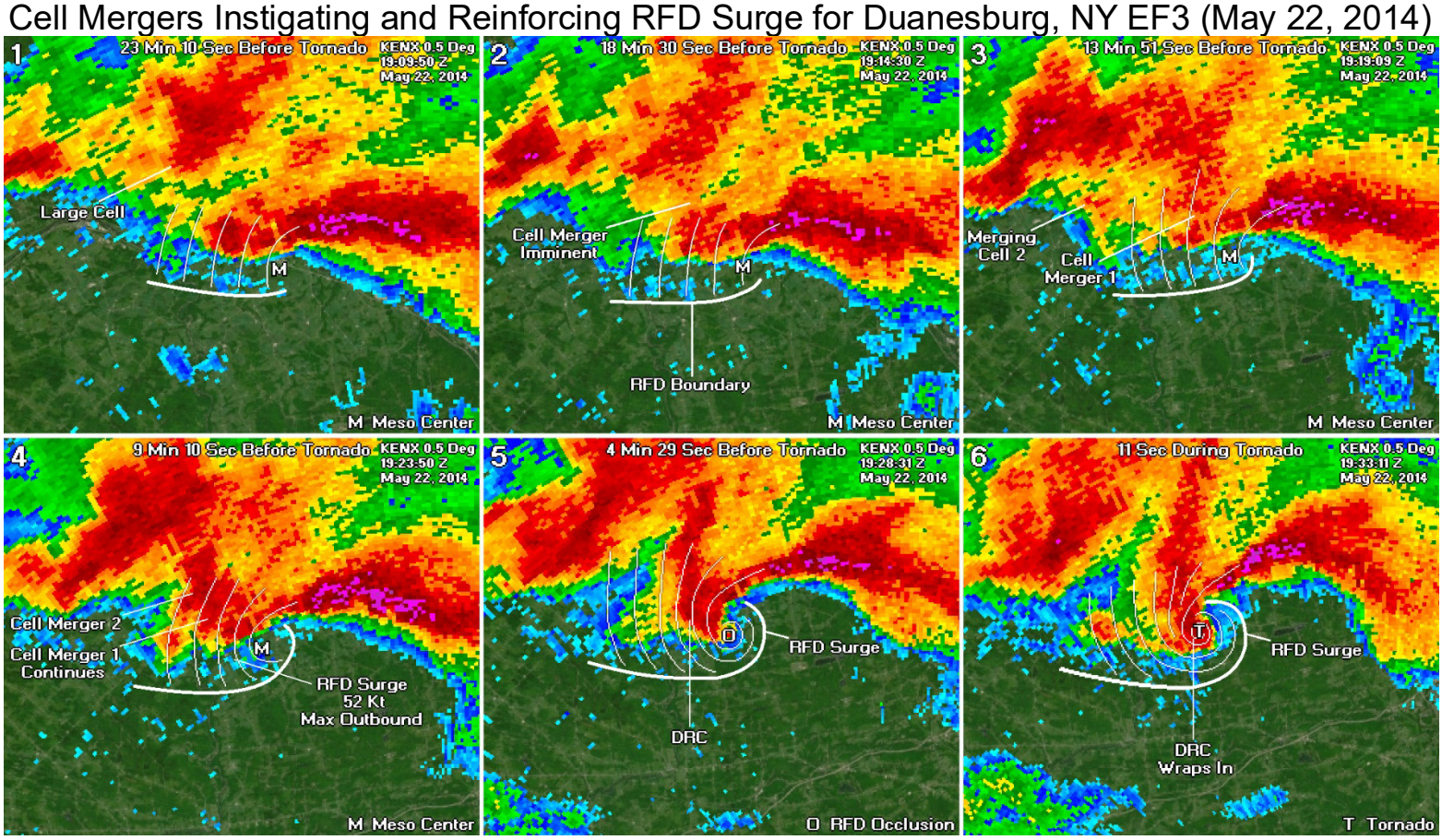

Figure 25. The RFD surge associated with the Duanesburg, New York EF3 tornado on May 22, 2014. This was a northwest mid-level flow case with a storm movement to the south-southeast. A large cell is evident to the northwest of the Duanesburg supercell in panel 1. This cell approaches and merges with the back edge of a large pendant extending westward from the Duanesburg supercell's main core, constituting cell merger one (panel 2 and 3). Cell merger one continues in panel 4, which results in a prominent RFD surge that takes place in panel 4, 5 and 6. Cell merger two has begun in panel 4, which instigates the DRC and reinforces the RFD surge. The RFD surge moves quickly eastward as the RFD occlusion forms well behind the RFD boundary (panel 5). The DRC wraps into the RFD occlusion as the tornado forms in panel 6.

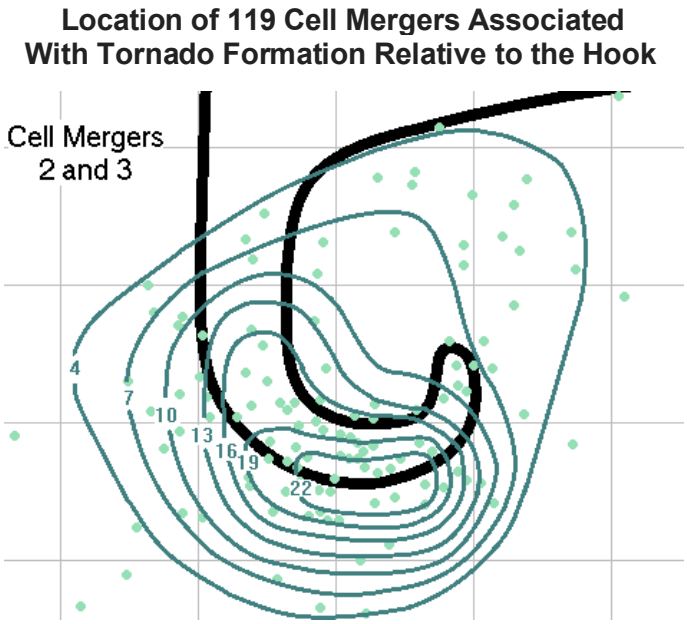

Figure 26. The locations of cell merger two and three for 119 cell mergers that took place during tornadogenesis from June 5, 2010 to March 15, 2012. The cell mergers are plotted relative to the hook. These cell mergers appeared to strengthen the RFD surge, the DRC or RFD occlusion prior to tornado formation.

Figure 26 shows a plot of the locations of 119 cell mergers (cell merger 2 and 3) identified from June 5, 2010 to March 15, 2012. This type of cell merger most often occurred on the south edge of the hook but could also occur anywhere around the hook and along the forward flank. The most important aspect was that the cell merger occurred close enough to the RFD occlusion to have an impact on tornadogenesis. Some cell mergers took over 15 minutes to merge, while fast moving smaller cells could merge in tens of seconds. This was determined using cell motion speeds, directions and interpolation analysis. And some cell mergers were large, while others were very small.

Figure 27 shows a group of cell mergers that happened on December 25, 2012. For this case, each of the three cell mergers took place close to the RFD occlusion. Each likely had an impact on tornadogenesis based on the close proximity to the RFD occlusion. These cell mergers likely infused strong winds into the RFD occlusion, enhancing vertical vorticity to aid tornado formation. A rapid increase in precipitation is evident in this case around the RFD occlusion just prior to tornado formation. This was a common theme among the 208 supercell cases.

In our database, the largest cell merger during tornadogenesis, occurred on May 24, 2011 with the forward flank of the El Reno EF5 tornadic supercell. The El Reno case, along with the large cell merger, is covered in Part 2 of this study. The El Reno cell merger is also examined in Tanamachi et al. 2015.

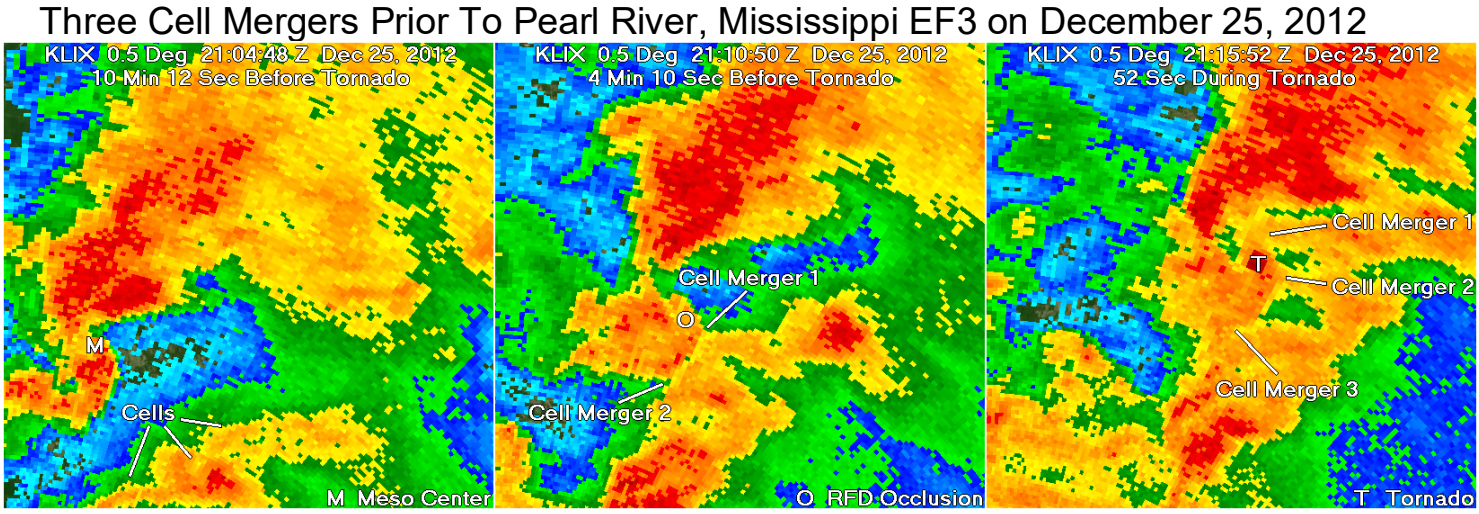

Figure 27. Three cell mergers that likely infused strong winds into the RFD occlusion, helping to increase vertical vorticity around the meso, from five minutes before the tornado to just after tornado development. This supercell produced the Pearl River, Mississippi EF3 tornado.

7. FINAL CONSIDERATIONS

While the 208 case database suggests that there are common features and characteristics preceding tornadogenesis, the process is no doubt very complex, as is presented in Kosiba et al. 2013 for the Goshen, Wyoming tornado on June 5, 2009. It is one thing to analyze tornadogenesis in a radar sequence, after the fact. But it is much more difficult to recognize the process occurring in real-time. Although tornadogenesis can be forecast in advance by keying in on environments associated with low LCL heights and strong low-level shear (Markowski and Richardson 2009), it can be very difficult to forecast a high-end tornado in the short term, such as on a time-scale of 10 to 20 minutes. While the amplification of vertical vorticity that makes the tornado develop is generally understood (P. Markowski 2019 personal communication), there is still a great amount of mystery that occurs on the storm-scale within and around the developing tornado. And there is no single theory that explains all the commonly observed features in tornadogenesis (Rotunno 1986).

Near the beginning of the project, Paul Markowski responded to one of our questions by stating,

"Given that a tornado is a region of high vertical vorticity, the initial development of vertical vorticity at the surface is a prerequisite for tornado formation. I think this is understood pretty well, and that understanding is that downdrafts/outflow/baroclinic vorticity generation/tilting are all crucial, as explained in previous emails, and perhaps most succinctly in either the Physics Today or Weatherwise articles I referred you to. The amplification of the vertical vorticity to tornado strength is also fairly well understood in a broad sense; it obviously involves vorticity stretching (convergence of M). And we obviously are pretty good at anticipating which environments this is all most likely to happen in (i.e., environments with low LCLs, strong low-level shear). But on a storm-by-storm basis, predictability is very limited, no doubt because of the multitude of things that can happen on the smallest scales that are virtually impossible to anticipate, such as DRCs, storm-storm interactions, changes on surface characteristics, and perhaps even things like storm-HCR interactions."

For tornadogenesis in supercells, an unstable RFD is more favorable for tornado formation, than a cool and stable RFD (Markowski et al. 2002). The main reason for this is that instability is associated with vertical motion. Because the tornado is generated in the downdraft laden RFD, the RFD must be relatively unstable in order to maintain strong near-surface vertical motion necessary for tornado formation. Although the RFD surge appears to be critical for the development of the RFD occlusion and tornado, an RFD surge that is cold and stable will likely not be favorable for tornadogenesis, even if it undercuts the low-level mesocyclone. The potential for tornadogenesis decreases as the RFD becomes negatively buoyant, which inhibits the stretching of outflow air (Kosiba et al. 2013). On the contrary, RFDs that are unstable are more efficient at producing low-level convergence, which is an important component to help rotation intensify (Markowski et al. 2003).

A second reason is that unstable RFDs are more likely to produce relatively low-topped cells that merge with the supercell's pendant. For the first 26 storms in the database, merging cells were estimated to be about half of the height of the supercell's main core, with an average estimated top elevation at 21,964 feet. The low tops enable the downdrafts in these merging cells to remain more unstable. Cell mergers associated with low-topped storms appear to instigate the RFD surge, which can create an inflow channel if the RFD surge is strong enough. Winds dramatically increase within the inflow channel, which leads to a strengthening of the low-level mesocyclone. Also, these low-topped cell mergers aid DRC development and merge with the RFD occlusion, helping to strengthen the column of vertical vorticity just prior to tornado formation.

8. CONCLUSION

For this study, 208 supercells that produced EF3 to EF5 tornadoes were analyzed. Average times were found concerning several key components of tornadogenesis.

For these cases, the rear flank downdraft appears to play a critical role in tornadogenesis. Prior to tornado formation, the surging rear flank downdraft was estimated to occlude for all 208 cases. Using the 208 case average, the RFD occlusion began just over 10 minutes prior to the tornado start time and ended just under 5 minutes prior to the tornado start time. This validates Robert Davies Jones' similar declaration that the RFD occlusion process occurs 5 to 10 minutes before the tornado (Davies-Jones 2006).

The position of the RFD boundary was estimated for all 208 cases relative to the tornado start location. 201 of 208 cases (96.6%) were located well to the west of the RFD boundary, while seven cases (3.4%) were located just inside the RFD boundary within one quarter of a nautical mile, or on the RFD boundary itself. On average, the tornado start location was 1.7 nautical miles to the west and 1.1 nautical miles to the south of the RFD boundary.

The distribution of tornado start location relative to the RFD boundary shows an axis of higher incidence located from near the RFD boundary extending southwestward across the northeastern quadrant of the RFD. On average, just prior to the start of the tornado, the RFD occlusion moved southwestward relative to the RFD. This was found to be due to the RFD surge, which pushes the RFD boundary toward the forward flank and further away from the strengthening circulation over time. Using the 208 case average, the RFD surge began over 13 minutes before the tornado start time and ended at just over 4 minutes after the tornado start time, having a duration of almost 18 minutes. On average, the RFD surge moved 7 knots faster than the speed of the supercell.

Cell merger one occurred on average 15 minutes prior to the tornado start time, appearing to instigate the descending reflectivity core and the RFD surge. A second cell merger occurred on average 7 minutes prior to the tornado start time. Cell merger two appeared to do the following: reinforce the RFD surge, aid DRC development and help vorticity to increase in the RFD occlusion. A third cell merger occurred on average just over 2 minutes prior to the tornado start time, likely helping to strengthen vertical vorticity within the RFD occlusion just prior to the tornado.

The RFD surge appears to be a critical component of tornadogenesis. The RFD surge pushes northeastward toward the forward flank, impinging upon the supercell's inflow sector, and creating an inflow channel, where radar estimates of these cases show wind speeds approximately double. A suspected pressure drop likely occurs from the inflow channel into the RFD's northeast quadrant due to the Bernoulli Effect, which strengthens the surface low and associated RFD occlusion. This also likely strengthens updraft speeds and intensifies the low-level mesocyclone. Second, it is hypothesized that the RFD pushes air with relatively less vertical shear beneath the low-level mesocyclone. Less vertical shear compared to that of the inflow sector, would make it easier for the low-level mesocyclone to stretch the column of vertical vorticity upward in order to create the tornado. And third, distance measurements on average for these cases show that the low-level mesocyclone moves deeper inside the RFD just prior to the tornado. This places the mesocyclone in close proximity to the descending reflectivity core, which has been found to be a critical player in tornadogenesis.

For questions about this study, please contact Chris Broyles at chris.broyles@noaa.gov.

9. ACKNOWLEDGEMENTS

We are extremely grateful to Israel Jirak for doing an excellent review of our papers. We are also thankful to the guidance that Patrick Skinner gave to us early on during our tornadogenesis project. Thanks also goes to John Hart and Brian Squitieri for giving guidance during the review process. Also, we are thankful to Paul Markowski and Jana Houser, who we consulted early in the project for guidance. Finally, we thank Ethan Broyles for giving us feedback concerning graphic presentation.

10. REFERENCES

Bluestein, H. B., and Weisman M. L. , 2000: The interaction of numerically simulated supercells initiated along lines. *Mon. Wea. Rev.*, **128 ,** 3128–3149.

Bluestein, H. B., J. C. Snyder, and J. B. Houser, 2015: A multiscale overview of the El Reno, Oklahoma, tornadic supercell of 31 May 2013. *Wea. Forecasting*, **30**, 525–552.

Davies-Jones, R. P., 1982: Observational and theoretical aspects of tornadogenesis. *Intense Atmospheric Vortices,* L. Bengtsson and J. Lighthill, Eds. Springer-Verlag, 175–189.

Davies-Jones, R. P., 2006: Tornadogenesis in supercell storms—What we know and what we don't know. Preprints, *Symposium on the Challenges of Severe Convective Storms,* Atlanta, GA, Amer. Meteor. Soc., 2.2.

Davies-Jones, R. P., R. J. Trapp, and H. B. Bluestein, 2001: Tornadoes and tornadic storms. *Severe Convective Storms,* C. A. Doswell, Ed., Amer. Meteor. Soc., 167–221.

Flournoy, M. D., A. Lyza, M. Satrio, M. Diedrichsen, M. Coniglio, and S. Waugh, 2022: A climatology of cell mergers with supercells and their association with mesocyclone evolution. *Mon. Wea. Rev.*, **150**, 451–461.

Fujita, T., 1975: New evidence from April 3-4, 1974 Tornadoes. SMRP Research Paper No. 127.

Hastings, R. M., Y. P. Richardson, and P. M. Markowski, 2014: Simulation of near-surface mesocyclogenesis during mergers between mature and nascent supercells. *27th Conf. on Severe Local Storms,* Madison, WI, Amer. Meteor. Soc., 3B.2.

Klemp, J. B., and R. Rotunno, 1983: A study of the tornadic region within a supercell thunderstorm. *J. Atmos. Sci.,* **40,** 359–377.

Kosiba, K. A., J. Wurman, P. Markowski, Y. Richardson, P. Robinson, and J. Marquis, 2013: Genesis of the Goshen County, Wyoming, tornado on 5 June 2009 during VORTEX2. *Mon. Wea. Rev.*, **141**, 1157–1181.

Kurdzo, J. M., Bodine D. J. , Cheong B. L. , and Palmer R. D. , 2015: High temporal resolution polarimetric X-band doppler radar observations of the 20 May 2013 Moore, Oklahoma Tornado. *Proc. 27th Conf. on Severe Local Storms,* Madison, WI, Amer. Meteor. Soc., 11A.3.

Lee, B. D., B. F. Jewett, and R. B. Wilhelmson, 2006: The 19 April 1996 Illinois tornado outbreak. Part II: Cell Mergers and associated tornado incidence. *Wea. Forecasting*, **21**, 449-464.

Lee, B. D., C. A. Finley, and C. D. Karstens, 2012: The Bowdle, South Dakota, cyclic tornadic supercell of 22 May 2012: Surface analysis of rear-flank downdraft evolution and multiple internal surges. *Mon. Wea. Rev.*, **140,** 3419–3441.

Lee, B. D., C. A. Finley, and T. M. Samaras, 2011: Surface analysis near and within the Tipton, Kansas, tornado on 29 May 2008. *Mon. Wea. Rev.*, **139**, 370–386.

Lemon, L. R. and C. A. Doswell, 1979: Severe thunderstorm evolution and mesocyclone structure as related to tornadogenesis. *Mon. Wea. Rev.*, 107, 1184-1197.

Lewellen, D. C., and W. S. Lewellen, 2007: Near-surface vortex intensification through corner flow collapse. *J. Atmos. Sci.*, **64**, 2195–2209.

Lewellen, D. C., and W.S. Lewellen, 2007: Near-surface intensification of tornado vortices. *Journal of the Atmospheric Sciences*, **64**, pp. 2176-2194

Markowski, P. A., 2002a: Hook echoes and rear-flank downdrafts: A review. *Mon. Wea. Rev.*, **130 ,** 852–876.

Markowski, P. N., Straka J. M. , and Rasmussen E. N. , 2002: Direct surface thermodynamic observations within the rear-flank downdrafts of nontornadic and tornadic supercells. *Mon. Wea. Rev.*, **130 ,** 1692–1721.

Markowski, P. M., J. M. Straka, and E. N. Rasmussen, 2003b: Tornadogenesis resulting from the transport of circulation by a downdraft: Idealized numerical simulations. *J. Atmos. Sci.*, **60**, 795–823.

Markowski, P., and Y. Richardson, 2009: Tornadogenesis: Our current understanding, forecasting considerations, and questions to guide future research. *Atmos. Res.*, **93**, 3–10.

Marquis, J. N., Y. P. Richardson, J. M. Wurman, and P. M. Markowski, 2008: Single- and dual-Doppler analysis of a tornadic vortex and surrounding storm scale f low in the Crowell, Texas, supercell of 30 April 2000. Mon. Wea. Rev.,136, 5017–5043.

Peters, J. M., C. Nowotarski, and H. Morrison, 2019b: The role of vertical wind shear in modulating maximum supercell updraft velocities. *J. Atmos. Sci.*, **76**, 3169–3189.

Rogers, J. W., 2012: Significant tornado events associated with cell mergers. *Preprints, 26th Conf. on Severe Local Storms*, Nashville, TN, Amer. Meteor. Soc., 9.4.

Rogers, J., and C. Weiss, 2008: The association of cell mergers with tornado occurrence. *Preprints, 24th Conf. on Severe Local Storms*, Savannah, GA, Amer. Meteor. Soc., P3.23.

Rotunno, R., . 1986: Tornadoes and tornadogenesis. *Mesoscale Meteorology and Forecasting,* P. S. Ray, Ed., 414–436.

Skinner, P. S., C. C. Weiss, L. J. Wicker, C. K. Potvin, and D. C. Dowell, 2015: Forcing mechanisms for an internal rear-flank downdraft momentum surge in the 18 May 2010 Dumas, Texas, supercell. *Mon. Wea. Rev.*, **143**, 4305–4330.

Skinner, P. S., C. C. Weiss, M. M. French, H. B. Bluestein, P. M. Markowski, and Y. P. Richardson, 2014: VORTEX2 observations of a low-level mesocyclone with multiple internal rear-flank downdraft momentum surges in the 18 May 2010 Dumas, Texas, supercell. *Mon. Wea. Rev.*, **142**, 2935–2960, doi:10.1175/MWR-D-13-00240.1.

Storm Data Publication, National Oceanic and Atmospheric Administration, National Centers for Environmental Prediction, https://www.ncdc.noaa.gov/stormevents/

Tanamachi, R. L., P. L. Heinselman, and L. J. Wicker, 2015: Impacts of a storm merger on the 24 May 2011 El Reno, Oklahoma, tornadic supercell. *Wea. Forecasting*, **30**, 501–524.

Wicker, L. J., and R. B. Wilhelmson, 1995: Simulation and analysis of tornado development and decay within a three-dimensional supercell thunderstorm. *J. Atmos. Sci.*, **52 ,** 2675–2703.

Wurman, J., Y. Richardson, C. Alexander, S. Weygandt, P. F. Zhang, 2007: Dual-Doppler and Single-Doppler Analysis of a Tornadic Storm Undergoing Mergers and Repeated Tornadogenesis. *Mon. Wea. Rev.*, **135**, 736-758.